Polycomb-dependent differential chromatin compartmentalization determines gene co-regulation in Arabidopsis

Ying Huang, Sanchari Sicar, Juan S Ramirez-Prado, Deborah Manza-Mianza, Javier Antunez-Sanchez, Rim Brik-Chaouche, Natalia y Rodriguez-Granados, Jing An, Catherine Bergounioux, Magdy M Mahfouz, et al.

Polycomb-dependent differential chromatin compartmentalization determines gene co-regulation in *Arabidopsis*

Ying Huang[1], Sanchari Sicar[1], Juan S. Ramirez-Prado[1], Deborah Manza-Mianza[1], Javier Antunez-Sanchez[2], Rim Brik-Chaouche[1], Natalia Y. Rodriguez-Granados[1], Jing An[1], Catherine Bergounioux[1], Magdy M. Mahfouz[3], Heribert Hirt[1,3], Martin Crespi[1], Lorenzo Concia[1, 4], Fredy Barneche[4], Simon Amiard[5], Aline V. Probst[5], Jose Gutierrez-Marcos[2], Federico Ariel[6], Cécile Raynaud[1], David Latrasse[1*] and Moussa Benhamed[*1,7,8]

1- Université Paris-Saclay, CNRS, INRAE, Univ Evry, Institute of Plant Sciences Paris-Saclay (IPS2), 91405, Orsay, France.
2- School of Life Science, University of Warwick, Coventry CV4 7AL, UK
3- Division of Biological and Environmental Sciences and Engineering, King Abdullah University of Science and Technology, Thuwal 23955-6900, Kingdom of Saudi Arabia
4- Institut de Biologie de l'Ecole Normale Supérieure (IBENS), ENS, CNRS UMR8197, INSERM U1024, PSL Research University, Paris, France.
5- GReD, Université Clermont Auvergne, CNRS, INSERM, BP 38, 63001, Clermont-Ferrand, France
6- Instituto de Agrobiotecnología del Litoral, CONICET, Universidad Nacional del Litoral, Colectora Ruta Nacional 168 km 0, 3000, Santa Fe, Argentina
7- Université de Paris, Institute of Plant Sciences Paris-Saclay (IPS2), F-75006 Paris, France.
8- Institut Universitaire de France (IUF).

* Correspondence to: DL (david.latrasse@u-psud.fr) and MB (moussa.benhamed@u-psud.fr)

Running title: H3K27me3 triggers repressive loop formation

Keywords: Chromatin architecture, Chromatin loops, Polycomb, Capture Hi-C, HiChIP

Abstract

In animals, distant H3K27me3-marked Polycomb targets can establish physical interactions forming repressive chromatin hubs. In plants, growing evidence suggests that H3K27me3 acts directly or indirectly to regulate chromatin interactions, although how this histone modification modulates 3D chromatin architecture remains elusive. To decipher the impact of the dynamic deposition of H3K27me3 on the *Arabidopsis thaliana* nuclear interactome, we combined genetics, transcriptomics and several 3D epigenomic approaches. By analyzing mutants defective for histone H3K27 methylation or demethylation we uncovered the crucial role of this chromatin mark in short- and previously unnoticed long-range chromatin loop formation. We found that a reduction in H3K27me3 levels led to a decrease in the interactions within Polycomb-associated repressive domains. Regions with lower H3K27me3 levels in the H3K27 methyltransferase *clf* mutant established new interactions with regions marked with H3K9ac –a histone modification associated with active transcription–, indicating that a reduction in H3K27me3 levels induces a global reconfiguration of chromatin architecture. Altogether, our results reveal that the 3D genome organization is tightly linked to reversible histone modifications that govern chromatin interactions. Consequently, nuclear organization dynamics shapes the transcriptional reprogramming during plant development and places H3K27me3 as a key feature in the co-regulation of distant genes.

Introduction

Gene expression regulation underlying eukaryotic cell differentiation depends largely on covalent modifications of nuclear chromatin, including histone modifications (Ahmad et al. 2010). It has been shown that histone modifications alter chromatin condensation, which ultimately affects global genome topology in the nucleus, as well as the local chromatin 3D conformation, thereby modulating the accessibility of specific loci to the transcriptional machinery (Rodriguez-Granados et al. 2016; Huang et al. 2020). In the last few years, the concept of genetic information encoded in a linear sequence of nucleotides associated with histones has evolved into a more comprehensive viewpoint considering the dynamic 3D architecture of the cell nucleus (Misteli 2007). From this perspective, structural elements such as *loops, domains, territories* and *factories* emerge as crucial functional features controlling the physical interaction between promoters and distant regulatory elements (Sutherland and Bickmore 2009), as well as the spatial organization of transcriptional hubs. Consequently, nuclear organization dynamics appear as an integrator of developmental and environmental signals (Huang et al. 2020).

The advent of innovative methods to study genome-wide 3D spatial chromatin organization from a molecular perspective, such as Hi-C, HiChIP, and ChIA-PET, has allowed to uncover both small- and large-scale genome architecture in various cell types of metazoan organisms, notably in mammals (Mishra and Hawkins 2017; Fullwood et al. 2009; Mumbach et al. 2016; Mifsud et al. 2015). This has revealed the existence of megabase-long chromatin compartments comprising either active (A compartment) or inactive chromatin (B compartment) (Dong et al. 2017b; Rowley et al. 2017; Fortin and Hansen 2015). Furthermore, it also allowed the identification of topologically associated domains (TADs) as fundamental units of 3D genome organization. TADs are large self-interacting genomic regions (Gonzalez-Sandoval and Gasser 2016; Rocha et al. 2015; Dixon et al. 2016, 2012), which encompass genes displaying similar expression dynamics, suggesting that physical association is functionally relevant for the control of transcriptional activity (Dekker and Heard 2015). Higher-resolution studies have shown

that TADs can be further-subdivided into compartmental domains which formation appears to be governed by transcription (Rao et al. 2017; Rowley et al. 2017).

Even though plant and metazoan nuclei share certain commonalities, they also display radical differences (Feng et al. 2014; Grob et al. 2014; Dong et al. 2017a; Mascher et al. 2017; Rodriguez-Granados et al. 2016; Huang et al. 2020). Notably, plants lack genes encoding CTCF transcription factors, which have been pointed in animals as key players in the establishment of TADs and chromatin loops (de Wit et al. 2015; Guo et al. 2015). Pioneer Hi-C analyses revealed the absence of TAD-like structures in *Arabidopsis thaliana* (Wang et al. 2015; Feng et al. 2014; Grob et al. 2014), a phenomenon that has been attributed to the small size of its compact genome, which exhibits relatively homogenous transcriptional rates and a low density of noncoding regions (Rowley and Corces 2016; Rowley et al. 2017). Recent studies in plants with large and complex genomes have revealed the existence of TAD-like domains (Liu et al. 2017; Wang et al. 2018; Dong et al. 2018; Concia et al. 2020; Dong et al. 2017a). However, unlike their animal counterparts, these TAD-like structures mainly correspond to large heterochromatic compartments, suggesting that they should rather be referred to as ICONS (Intergenic CONdensed Spacers), as they are not functionally equivalent to TADs (Huang et al. 2020 ; Concia et al. 2020).

The existence of a large repertoire of histone modifications and variants with distinct physical properties and associated to diverse chromatin states (e.g. constitutive heterochromatin, facultative heterochromatin, euchromatin), allows the establishment of a highly precise cell-specific transcriptional landscape in response to environmental and developmental stimuli (Kouzarides 2007; Eichten et al. 2014). The numerous changing environmental signals perceived by the cell require a pertinent response, which must be accurately modulated with time (Gambino and Pantaleo 2017). Thus, reversible and dynamic histone modifications permit the induction and repression of the appropriate subsets of genes under certain conditions (Pfluger and Wagner 2007). In agreement, protein complexes and enzymes with opposite activity upon histone covalent modifications continuously shape the chromatin environment of

target genes. Thus, the so-called *writers* govern the deposition of a specific covalent histone modification, while *erasers* participate in their removal (Mach 2018). A third group of proteins called *readers,* recognizes specific histone modifications and induces downstream processes through diverse mechanisms, including chromatin compaction, remodeling, the recruitment of secondary chromatin modifiers, Transcription Factors (TF) and the DNA damage repair machinery, among others (Yun et al. 2011).

The tri-methylation of the lysine 27 of histone H3 (H3K27me3) is a repressive covalent histone modification resulting from the activity of Polycomb Repressive Complexes (PRCs), formed by the combination of multiple Polycomb group (PcG) proteins (Grossniklaus and Paro 2014). In both animals and plants, PRCs are classified into PRC1 and PRC2, in which PRC2 deposits H3K27me3 on its targets, while PRC1 recognizes these histone modifications and stabilizes PRC2-mediated repression. There are three SET-domain proteins with H3K27me3 methyltransferase activity in *Arabidopsis thaliana*: SWINGER (SWN), CURLY LEAF (CLF) and MEDEA (MEA) (Mozgova et al. 2015). The PcGs activity in this plant model is counteracted by four Jumonji (JMJ)-type proteins, which perform the active demethylation of H3K27me3 and determine spatial boundaries for this histone modification, restricting its spreading and the consequent formation of repressive chromatin domains (Yan et al. 2018). Among them, REF6 (RELATIVE OF EARLY FLOWERING 6) has been reported to promote flowering through the activation of the flower integrators *FT* (*FLOWERING LOCUS T*) and *SOC1* (*SUPRESSOR OF CO OVEREXPRESSION 1*) (Hou et al. 2014; Noh et al. 2004). Moreover, the *ref6* mutation partially complements the developmental phenotype and the decreased fertility caused by the *clf* mutation (Lu et al. 2011). Consistently, the *REF6* over-expressing plants share several of the developmental phenotypes of *clf*, highlighting the antagonistic function between this protein and the PRC2 complex (Lu et al. 2011).

Growing evidence indicates that H3K27me3 plays an important role in the spatial organization of chromatin in eukaryotes, a phenomenon that has been associated with its repressive role in

transcription. For instance, it has been shown in animals that Polycomb targets marked with H3K27me3 can establish interactions between them, forming repressive chromatin hubs dependent on PRCs and insulator proteins (Lanzuolo et al. 2007; Cheutin and Cavalli 2014). PRCs have also been shown to regulate the maintenance of pluripotency in mammalian embryonic stem cells through the organization of interaction networks (Schoenfelder et al. 2015), and H3K27me3 levels have been associated with the *Drosophila*'s genome subdivision into TADs (El-Sharnouby et al. 2017 ; Boettiger et al. 2016; Eskeland et al. 2010; Francis et al. 2004; Joshi et al. 2015; Kundu et al. 2017; Williamson et al. 2012; McLaughlin et al. 2019). In plants, several studies suggested that this covalent histone modification is a key contributor to chromatin topology. A Hi-C approach served to propose that the local interaction of H3K27me3 domains is reduced in the *Arabidopsis clf*/*swn* double mutant background (Feng et al. 2014). Besides, it has been shown that H3K27me3 is enriched at long-distance interacting loci across the *Arabidopsis* genome (Liu et al. 2016a). Furthermore, in a previous study, we showed that the *Drosophila* HETEROCHROMATIN PROTEIN1 (HP1) homolog in *Arabidopsis* LIKE-HP1 (LHP1) participates in the 3D-conformation of the *Arabidopsis* genome (Veluchamy et al. 2016), and that its genome-wide distribution perfectly matches that of H3K27me3. LHP1 is considered a component of the plant PRC1 complex, given its capacity to recognize H3K27me3 through its chromodomain (Gaudin et al. 2001; Turck et al. 2007; Zhang et al. 2007). Therefore, H3K27me3 may directly or indirectly participate in the regulation of the dynamic interactivity of Polycomb target genes. However, several aspects of the molecular function of H3K27me3 in 3D chromatin architecture determination remain unclear. In order to gain a deeper understanding of the molecular role of H3K27me3, we combined cutting-edge technologies applied to the characterization of 3D chromatin conformation.

Results

Arabidopsis chromatin organization displays a strong compartmentalization

154 The first Hi-C analyses performed in *Arabidopsis* nuclei revealed that TADs, which are widely distributed
155 among metazoans and plants, are hardly found (Liu et al. 2016a). Long-range chromatin interactions are
156 rare in this organism and correspond almost exclusively to heterochromatic regions such as
157 centromeres. A notable exception of this phenomenon is the KNOT, which brings together
158 heterochromatic islands within euchromatin (Grob et al. 2014).
159 In order to determine the extent to which chromatin compartmentalization is a characteristic feature of
160 the *Arabidopsis* genome, we performed immuno-detection of H3K27me3 and H3K9ac, two histone post-
161 translational modifications associated to gene repression and activation, respectively. The immuno-
162 staining performed on somatic nuclei during interphase revealed a heterogeneous distribution of these
163 covalent histone modifications, suggesting that distinct euchromatin and facultative heterochromatin
164 compartments exist in *Arabidopsis* (Fig. 1A and Supplemental Fig. S1). Moreover, by measuring the
165 H3K9ac and H3K27me3 signal distribution along a virtual axis arbitrarily defined in an immuno-stained
166 nucleus, we observed that the corresponding peaks are anti-correlated (Fig. 1B). Given the proximity
167 between H3K9ac and H3K27me3 marked genes along the chromosome and the resolution of the
168 confocal microscope that is about 0.5µm, this result suggest that actively transcribed and repressed
169 genes occupy distinct compartments within the cell nucleus. To gain a deeper understanding of the
170 compartmental organization of active and silent chromatin, we conducted HiChIP, a sensitive method for
171 the efficient analysis of protein-centric chromosome conformation (Fig. 1C, 1D and Supplemental Fig. S2)
172 (Mumbach et al. 2016). H3K27me3- and H3K9ac- HiChIPs were performed in 14-day-old wild-type (WT)
173 shoots. A minimum of 159 million of read pairs were produced for each sample, and 116 million uniquely
174 mapped read pairs were generated (Supplemental Table S1), with a high reproducibility between
175 replicates (Supplemental Fig. S3). In parallel, ChIP-seq was performed for the same histone
176 modifications. In contrast to traditional Hi-C (Fig. 1C and 1D, left panels), the HiChIP approach allows
177 revealing interactions associated with each specific histone modification (Fig. 1C and 1D, right panels).

Both short- and long-range interactions from few kilo-bases to several mega-bases were detected at the site of the respective histone modifications (Supplemental Fig. S4 and Supplemental Table S2, S3, S4 and S5). By overlapping both H3K9ac and H3K27me3 HiChIP signals, our data suggested that genes associated to the same histone modification interact with each other to form contact domains and fold the genome locally to allow the spatial segregation of transcriptionally active and silent chromatin (Fig. 1E).

Shoot and root nuclei display distinct 3D chromatin architecture

The 3D configuration of the nuclear genome is non-random and correlates with cell type-specific transcriptomes; however, the mechanisms implicated in the establishment of this configuration are poorly understood in plants. It has been recently shown that biosynthetic non-homologous gene clusters are embedded in local 3D configurations that segregate cluster regions from the surrounding chromosome environment. Based on Hi-C and H3K27me3 distribution in *Arabidopsis*, it has been proposed that genome topology differs between shoots and roots (Nützmann et al. 2020). In order to further decipher the relationship between H3K27me3 and 3D chromatin conformation, we performed H3K27me3- HiChIP and ChIP-seq in shoots and roots. The high-resolution interaction matrix obtained by HiChIP revealed the widespread presence of interactions between genomic bins including H3K27me3-enriched genes from both tissues (Supplemental Fig. S5 and S6). A differential analysis using HOMER comparing shoots and roots served to identify the most informative loops associated with H3K27me3 (Fig. 2A), which allowed us to focus on the top shoot-specific repressive loops (SSRLs) in downstream analyses (Supplemental Table S6). We found a positive correlation between H3K27me3 levels and the strength of the detected interactions when SSRLs were visualized at different scales (Fig. 2B and 2C). To further support our observations, we quantified the level of this histone modification in shoots and roots on genes associated to SSRLs, and observed that 47% of those genes are hypermethylated in shoot

compared to root, confirming that this repressive histone modification is associated with chromatin loop formation and/or stability (Fig. 2D and Supplemental Table S7).

We then wondered whether gene pairs connected in SSRLs show similar changes in expression levels between shoots and roots. Using publicly available gene expression data (Liu et al. 2016b), we plotted the top SSRL gene pairs using the $\log_2$ (fold-change shoot/root) of the first gene as the predictor and the $\log_2$ (fold-change shoot/root) of the second gene as the response (Fig. 2E, Supplemental Fig. S7 and Supplemental Table S8). This analysis revealed a significant correlation between H3K27me3 SSRL-associated loci and genes repressed in shoots (Fig. 2E). These data indicate that genes displaying specific physical contacts, and associated with H3K27me3, exhibit similar transcriptional behavior and are likely part of common Polycomb-repressive compartments (Fig. 2E).

It has been extensively shown that H3K27me3 works as a repressive covalent histone modification participating in the regulation of multiple developmental genes in plants (Cheng et al. 2020). Then, to better understand the impact of H3K27me3-dependent chromatin architecture on plant development, we performed an analysis of Gene Ontology (GO) terms enriched among loci grouped in SSRLs with a lower expression in shoots than in roots. We found a significant enrichment in GO categories related to root development and cell identity (Fig. 2F), hinting at a comprehensive epigenetic reprogramming of developmental pathways in different organs. Reciprocally, we also explored the root specific repressive loops (RSRLs) and their impact on developmental outputs (Fig. 2G and Supplemental Table S9). In agreement with our observations for SSRLs, genes associated in RSRLs displayed higher H3K27me3 levels in roots than in shoots and lower expression levels in roots compared to shoots (p-value = 3.2E-55) (Fig. 2G-K, Supplemental Fig. S7, Supplemental Table S10 and S11). In addition, the GO analysis of genes grouped in RSRLs, which are down regulated in roots, showed enrichment in categories related to shoot development and photosynthesis (Fig. 2L), in agreement to the non-photosynthetic nature of root tissues. These observations suggest a role of H3K27me3-dependent genome topology in coordinating the

transcriptional activity underlying developmental programs.

One limitation of HiChIP when using antibodies directed against a particular histone modification, is that the detection of chromatin contact relies on the presence of this given histone modification at the site of interaction. Thus, the observed reduction of the strength of some interactions could merely reflect H3K27me3 depletion at loci of interest. To rule out this possibility, we performed capture-Hi-C (C-Hi-C). This approach combines Hi-C with the hybridization-based capture of targeted genomic regions (Supplemental Fig. S8). To this end, we generated a biotinylated RNA bait library specifically targeting 4,650 regions that accumulate H3K27me3 and included a subset of loci differentially methylated between shoots and roots (Supplemental Fig. S9). The comparison of both Hi-C and C-Hi-C matrixes allowed us to identify a significant enrichment of chromatin contacts over our target sequences (Fig. 3A) and to obtain a high-resolution map of interactions between captured regions, as well as between captured and non-captured regions (Fig. 3B). A differential analysis using HOMER resulted in the identification of 7,676 shoot-specific loops (SSLs), of which 277 overlapped with the SSRLs previously identified by HiChIP. These data suggest that the deposition of H3K27me3 participates in the establishment of tissue-specific chromatin loops (Fig. 3C-E and Supplemental Table S12, S13 and S8). Focusing on these SSLs identified by both methods, we found that 67% of the genes grouped in SSLs were found to be specifically repressed in shoots compared to roots (Fig. 3F). This proportion is significantly higher than the one expected by chance (p-value = 1.61E-144) (Supplemental Fig. S10). On the other hand, we found through the same approach 6737 root specific loops (RSLs), among which 231 were also found on the previously generated H3K27me3-HiChIP data analysis and defined RSRLs (Fig. 3G, 3H and 3I and Supplemental Table S13, S14). 54% of the genes grouped in RSLs were specifically repressed in roots compared to shoots, a proportion significantly higher than the one expected by chance (p-value = 2.71E-68) (Fig. 3J and Supplemental Fig. S10). We also observed that 24% and 35% of the genes respectively grouped in SSLs and RSLs displayed an unexpected behavior, what could be

explained by the fact that both shoots and roots correspond to complex samples of a mixture of various cell types. Altogether, our C-Hi-C data further supported that the H3K27me3 levels mediate the establishment and/or stability of repressive domains bringing together several genes in *Arabidopsis* and that Polycomb-related repressive compartments could play an important role in the transcriptional reprogramming underlying plant cell fate and organ development.

Ectopic deposition of H3K27me3 leads to occurrence of novel chromatin repressive loops

To decipher the impact of H3K27me3 levels on chromatin loop dynamics, we used the loss-of-function *ref6-5* mutant, defective for a histone demethylase and displaying ectopic accumulation of H3K27me3 at thousands of loci (Antunez-Sanchez et al. 2020; Lu et al. 2011; Yan et al. 2018) (Fig. 4A). Thus, in order to assess if ectopic H3K27me3 deposition could lead to the formation of new repressive compartments, we performed a C-Hi-C experiment comparing *ref*6-5 and WT shoots (Fig. 4B-D and Supplemental Fig. S11). A HOMER differential analysis identified the top *ref6*-Specific repressive Loops (reSLs) ranked according to the log fold-change and Z score (Fig. 4B and Supplemental Table S15). We observed that a large proportion of genes involved in reSLs displayed a significant increase in H3K27me3 levels in *ref*6-5 compared to WT (p-value = 4.62E-76) (Fig. 4C-E, Supplemental Fig. S12 and Supplemental Table S16). To confirm this, we assessed the proportion of *ref*6-5 hyper-methylated genes associated to repressive loops and found that 40% were associated with reSLs (Fig. 4C-D and Fig. 4E). These data suggest that a gain in H3K27me3 triggers the establishment of novel chromatin interactions (Fig. 4D). Using publicly available transcriptomic data (Antunez-Sanchez et al. 2020) we assessed whether gene pairs connected through reSLs showed similar transcriptional shifts between *ref6-5* and WT. We found a significant enrichment of co-repressed reSL-paired genes loci among the 546 plotted couples (p-value = 4E-10) (Fig. 4F, Supplemental Fig. S12 and Supplemental Table S17). This result indicates that genes displaying specific physical contact in *ref*6-5 are globally repressed, likely linked to the ectopic accumulation

H3K27me3 and the formation of repressive chromatin loops.

Reduction of H3K27me3 level induces a reconfiguration of chromatin architecture

Considering that the ectopic deposition of H3K27me3 induces the formation of novel chromatin repressive loops, we decided to assess the impact of a reduction in H3K27me3 deposition on the interaction profile within Polycomb-related repressive domains. To this end, we used *clf-29*, a Polycomb Repressive Complex 2 (PRC2) histone methyltransferase mutant that displays a strong reduction on H3K27me3 levels at thousands of loci (Veluchamy et al. 2016) (Fig. 4A). C-Hi-C and a differential analysis comparing *clf-29* and WT shoots identified the top *clf* Specific Disrupted Loops (cSDLs) ranked according to the log fold-change and Z score (Fig. 5A, 5B, Supplemental Fig. S13 and Supplemental Table S18). We observed that 33% of genes involved in cSDLs displayed a significant decrease in H3K27me3 levels in the *clf-29* mutant compared to WT (p-value = 9.72E-52) (Fig. 5C, 5D, Supplemental Table S19). To confirm this observation, we assessed the proportion of *clf* hypo-methylated genes associated to cSDLs and found that 40% of the *clf* hypo-methylated genes are associated to a cSDL, suggesting that the loss of H3K27me3 induced a destabilization of repressive loops in the *clf-29* (Fig. 5E). To uncover the impact of chromatin architecture reorganization on transcriptional reprogramming, we analyzed the expression of gene pairs normally brought together into spatial proximity in WT shoots, which are no longer clustered in the *clf-29*. We observed a significant enrichment in transcriptionally activated genes (p-value = 4.336E-7) (Fig. 5G, Supplemental Fig. S14 and Supplemental Table S20), indicating that genes involved in loops lost in the *clf-29* mutant tend to be upregulated. Altogether, our results suggest that a *clf*-dependent decrease in H3K27me3 leads to a re-configuration of chromatin architecture and the destabilization of H3K27me3-mediated repressive loops (Fig. 5B and 5F). This phenomenon can be associated to the transcriptional de-repression of hundreds of genes in PRC2-related mutants.

To better understand the association between genome topology reconfiguration, H3K27me3 deposition

and gene expression, we compared epigenomic and transcriptional features found in *clf-29* and WT, and integrated these datasets with chromatin interaction positioning (Supplemental Table S21). Our analysis revealed that interactions occur more frequently between genes with concordant transcriptional status, independently of whether they are up- or down-regulated in *clf-29* compared to the WT (Fig. 5G and 5H). Moreover, a similar trend was observed for the epigenomic profile, since genes with concordant H3K27me3 levels are more prone to interact in common hubs (Fig. 5G and 5H). A higher frequency in the interaction among hypomethylated genes in *clf-29* suggested a gain of novel interactions. Considering that *clf*-hypomethylated genes exhibited a global transcriptional activation, we assessed in WT shoots the distribution of the H3K9ac histone modification, characteristic of active loci. Then we mapped the gained interactions determined by C-Hi-C in *clf-29* throughout the genome, together with the distribution of the H3K9ac histone modification in the WT. We observed that regions losing H3K27me3 in *clf-29* tend to establish novel interactions with regions marked with the active histone modification H3K9ac (Fig. 5I and 5J, Supplemental Fig. S15 and S16, Supplemental Table S22, S23 and S24). This suggests that a reduction in H3K27me3 levels induces a global reconfiguration of chromatin architecture (Fig. 5J and 5K), allowing genes that lost their repressive covalent histone modification to integrate transcriptionally active hubs. Altogether, our results demonstrate that the 3D genome organization is tightly linked to histone modifications that dynamically modulate the determination of chromatin domains associated with gene co-regulation, thereby allowing the progression of plant developmental programs. Collectively, our data supports the view that H3K27me3 acts as a key regulator of global and local facultative heterochromatin topology in plants.

Discussion

The first analyses of the 3D genome organization of *Arabidopsis* revealed the absence of TAD structures and the existence of an “A/B” type compartmentalization at a local level, in domains of a few tens of kb

(Lieberman-Aiden et al. 2009; Grob et al. 2014). Constitutive heterochromatin, which contains mainly transposable element marked by specific histone modifications such as H3K9me2 and H3K27me1, is one of the major factors directing this compartmentalization. However, the contribution of facultative heterochromatin to higher-order nuclear topology in plants is not clearly stated. In the current study, through the integration of immuno-staining experiments and confocal microscopy, we provide evidence that H3K9ac-rich (euchromatin) and H3K27me3-rich (facultative heterochromatin) regions are spatially segregated, confirming that actively transcribed and repressed genes occupy distinct region in the nucleus. This result is consistent with previous ChIP-based studies in *Arabidopsis*, which have shown that the distribution of facultative heterochromatic histone modifications such as H3K27me3 on the linear genome is anti-correlated to euchromatic histone modifications (Ha et al. 2011).

Hi-C data is useful for the depiction of the genome-wide 3D organization of chromatin in the nucleus; however, to understand which proteins or covalent histone modifications have a role in structuring this organization, it is necessary to integrate it with external datasets (e.g. ChIP-seq) allowing only correlative analyses. To circumvent this limitation and to address whether and how genomic regions associated to histones bearing a specific covalent modification interact through long-range chromatin looping in a genome-wide and unbiased manner, we performed HiChIP experiments, confirming that transcriptionally active and inactive genes localize in different nuclear compartments. In addition, we also observed both long- and short-range interactions –ranging from a few kilo bases several mega bases –enriched at the site of either H3K27me3 or H3K9ac, highlighting the role of these histone modifications in 3D chromatin architecture. In plants, it has been previously hypothesized that H3K27me3 contributes to the establishment of chromatin loops, as this histone modification has been detected in interacting genomic regions (Liu et al. 2016a); however, in the current study we have taken advantage of the specific capture of H3K27me3-labeled chromatin loops to provide evidence of the role of this covalent histone modification in the spatial organization of chromatin. A similar approach has been used in maize to

346 identify *cis*-regulatory elements, revealing that H3K27me3 is potentially implicated in mediating
347 chromatin loops between regulatory elements and their target genes, in a process associated to gene
348 repression (Ricci et al. 2019).
349
350 **Chromatin architecture and development**
351 In the last few years, we have witnessed a significant increase in studies addressing the role of 3D
352 genome organization in the regulation of developmental processes as well as in response to
353 environmental cues. Hence, it is currently known that chromatin topology is highly dynamic during
354 animal developmental phase transitions, including gametogenesis, embryo development and cell
355 differentiation. The recent development of single-cell and low-input Hi-C approaches has permitted the
356 characterization of the embryo along different developmental stages, as well as different cell lines during
357 differentiation and lineage commitment. This has allowed to identify commonalities and particularities of
358 each cell type and to associate them to specific phenotypes (Zheng and Xie 2019). These single-cell
359 techniques have seldom been applied in plants, mainly due to the technical limitations that this imposes
360 (Huang et al. 2020); however, some studies have started characterizing the chromatin topology of
361 specific plant cell types, showing that as in animals, gamete, zygote and differentiated cells present
362 striking differences in their nuclear 3D chromatin configuration. By integrating single-cell 3C and Hi-C
363 approaches, Zhou and collaborators analyzed the 3D genomes of rice sperm, egg, unicellular zygote and
364 mesophyll cells, finding that rice nuclei present spatially organized chromatin territories associated to
365 different histone modifications and gene expression levels, providing evidence of the contribution of the
366 spatial organization of chromatin to the co-regulation of gene expression (Zhou et al. 2019).
367 The relevance of chromatin organization in the developmental context can be evidenced in the variety of
368 diseases and developmental problems that have been associated to abnormalities in chromatin
369 organization in various organisms. For instance, cardiac diseases, cancer and developmental disorders

have been attributed to mutations in genes encoding CTCFs and cohesion proteins (Rosa-Garrido et al. 2017; Kaiser and Semple 2017; Lupiáñez et al. 2015, 2016). Furthermore, the disruption of TAD boundaries has been shown to have developmental effects as a consequence of *enhancer hijacking,* or the abnormal interaction between an enhancer and a promoter. Several examples of this phenomenon have been reported in the literature (Zheng and Xie 2019; Kaiser and Semple 2017; Lupiáñez et al. 2016), highlighting the crucial role of chromatin organization on cell homeostasis and animal development. However, studies demonstrating the developmental consequences of chromatin disorganization in plants remain scarce. It has been recently shown that loss of CROWDED NUCLEI (CRWN) proteins, which are candidate nuclear lamina proteins in *Arabidopsis*, leads to a general reduction on chromatin organization and an associated reprogramming of the transcriptome (Choi et al. 2019; Hu et al. 2019). Furthermore, the loss of these proteins has been reported to induce dwarfism and a spontaneous cell death phenotype, which have been attributed to the constitutive induction of the salicylic acid-dependent pathway of immunity (Hu et al. 2019). These results suggest that as in animals, 3D chromatin organization plays a key role in the regulation of plant development and homeostasis. Furthermore, these results suggest that several of the pleiotropic phenotypes observed in plants defective in the epigenomic machinery may result from distortions in chromatin architecture and their impact on gene expression; however, this needs to be experimentally assessed.

In the current study we provide evidence for the existence of distinctive chromatin architecture between root and shoot cells, as evidenced by the presence of shoot- and root-specific repressive loops, mediated by H3K27me3. This represents valuable evidence for the understanding of how chromatin modifications contribute to chromatin topology and, consequently, to organ identity in plants. Our data shows that genes involved in SSRLs and RSRLs are associated with biological functions specific to the studied organs, supporting the view that chromatin loops contribute to the developmental differentiation of specific cells types in plants (Fig. 6).

Polycomb-repressed chromatin is critical for 3D nuclear organization in plants

Traditionally, Polycomb complexes have been associated to the repression of developmental genes, including the well described *Hox* genes (Bantignies et al. 2011; Kassis et al. 2017). However, the introduction of 3D epigenomic techniques has allowed to depict some of the molecular mechanisms by which these complexes regulate development, including the modulation of chromatin architecture (Pachano et al. 2019; Illingworth 2019). For instance, a recent study unveiled that H3K27me3 is a fundamental player in the chromatin reorganization occurring during oocyte development in mice (Du et al. 2020). Polycomb-Associated Domains (PADs) are self-interacting, cohesion-independent compartments enriched in H3K27me3 that are gradually established on the maternal genome until a late-stage before disappearing upon meiotic resumption. Hi-C analyses of mutants defective on PRC2 and PRC1 subunits revealed that PAD establishment is highly dependent on these complexes and H3K27me3 (Du et al. 2020). Most of the studies on the 3D organization of PcG-bound chromatin in mammals have been performed in embryonic stem cells (ESCs), and have illustrated that Polycomb proteins and their associated histone modifications accumulate in ESCs in discrete foci that have been named *PcG bodies* (Bantignies et al. 2011; Pachano et al. 2019). Mutations in subunits of both PRC2 and PRC1 have been shown to lead to the dispersion of these structures (Hernández-Muñoz et al. 2005), suggesting significant changes in chromatin architecture in these mutants. The molecular mechanisms connecting H3K27me3 deposition, loop formation and gene expression have been dissected into detail in *Drosophila*. This study showed (i) that H3K27me3 deposition is critical for loop formation and (ii) that chromatin looping contributes to gene repression, although it is not strictly required (Ogiyama et al. 2018). These results are coherent with our previous characterization of the *Arabidopsis lhp1* mutant, deficient in a PRC1 subunit, where a vast proportion of genomic interactions are lost (Veluchamy et al. 2016). The loss of these interactions is associated, to a large extent, to a significant reduction on H3K27me3 levels on interacting partners, suggesting that both LHP1 and H3K27me3 are involved in loop

formation in this organism. Since LHP1 is an H3K27me3 reader, it is considered to act, at least partially, downstream of H3K27me3 methyltransferases (Berry et al. 2017). Hence, if LHP1 activity depends on H3K27me3 levels, altering the latter through mutations on *CLF* or *REF6* should have an impact on chromatin looping. In agreement, in the current study we found that increasing H3K27me3 levels leads to the formation of new chromatin repressive loops, while reducing them has the inverse effect. Altogether, these results indicate that, similar to animals, PRCs and H3K27me3 play a fundamental role in the shaping of regulatory chromatin interactions and overall, chromatin conformation in the three-dimensional space, a phenomenon that is associated with developmental processes and, most likely, cell identity. However, the respective importance of H3K27me3 deposition and H3K27me3-mediated chromatin looping for efficient gene repression will require further investigation.

We found that some of the regions that lose H3K27me3 in the *clf* mutant tend to establish interactions with transcribed regions marked with H3K9ac. This may indicate that one of the mechanisms by which H3K27me3 contributes to gene repression is through the preclusion of these interactions. In addition, in animals, there is recent evidence indicating that histone hyperacetylation also contributes to nuclear organization, as it induces the formation of long-range chromatin interactions and nuclear sub-compartments (Rosencrance et al. 2020). This shows that the dynamic chromatin topology in the nuclear space results from the delicate balance of a plethora of elements, including various histone modifications, which recruit the nuclear machinery for its spatial organization. It has been proposed that nuclear proteins can pull the genome into new positions like in the game "cat's cradle", where the shape of a string is successively changed by opening up new sites for finger placement (Melé and Rinn 2016). Future research is likely to provide exciting new insights into the mechanisms involving histone modifications and associated molecules in the dynamic configuration of the plant genome.

In summary, our results demonstrate the 3D organization of the genome is tightly linked to histone modifications that trigger the formation of chromatin interactions associated to gene co-regulation. By

these means, they contribute to proper plant development, a process in which H3K27me3 is a key regulator of global and local facultative heterochromatin topology.

Methods

Plant material and growth conditions

Plant lines used in this study were in *Arabidopsis thaliana* ecotype Columbia (Col-0) background. The T-DNA insertional mutants *clf-29* (SALK_N521003) and *ref6*-5 mutant (GABI_705E03) was obtained from the GABI-Kat collection (Mirouze et al. 2012) were used. Seeds were surface-sterilized by treatment with bayrochlore, washed, and then sown in sterile half-strength MS medium, placed for 2–4 days at 4 °C to obtain homogeneous germination, and plants were grown in a vertical orientation in square petri dishes in growth chambers at 20 °C under long-day (16 h of light) conditions.

Immunostaining

Immunofluorescence labelling was performed according to Latrasse et al (Latrasse et al. 2017). Briefly, seedlings of 14-day-old *Arabidopsis* were fixed and then nuclei were isolated, placed on a poly-lysine slide and incubated overnight at 4 °C with primary antibodies specific to lysine-9-acetylated H3 (Millipore 07-352) and lysine-27-trimethylated H3 (Millipore 07-449). After washing, slides were incubated for 1h at room temperature in the dark either with Goat anti-Rabbit Alexa Fluor Plus 488 (A11034 Invitrogen) and Goat anti-Mouse Alexa Fluor Plus 555 (A32727 Invitrogen) or with Goat anti-Rabbit Alexa Fluor Plus 555 (A32732 Invitrogen) and Goat anti-Mouse Alexa Fluor Plus 488 (A32723 Invitrogen) as secondary antibodies. DNA was counterstained with 4,6 diamidino-2-phenylindole (DAPI) in SlowFade Diamond Antifade mounting media. Slides were directly imaged on a confocal microscope (Zeiss Microsystems).

Chromatin Immunoprecipitation followed by high-throughput sequencing (ChIP-seq) assay

ChIP-seq assays were performed on shoot or root of 14-day-old seedlings using anti-H3K27me3

(Millipore 07–449). Plant material was cross-linked in 1% (v/v) formaldehyde at room temperature for 15 min. Cross-linking was quenched with 0.125 m glycine for 5 min. The cross-linked plantlets were ground and nuclei were isolated and lysed in Nuclei Lysis Buffer (0,1% SDS, 50 mm Tris-HCl pH 8, 10 mm ethylene diamine tetraacetic acid (EDTA) pH 8). Cross-linked chromatin was sonicated for 5 min using a Covaris S220 (Peak Power: 175, cycles/burst: 200. Duty Factory: 20). The complexes were immunoprecipitated with antibodies, overnight at 4°C with gentle shaking, and incubated for 1 h at 4°C with 40 µl of Dynabeads Protein A (Thermo Fisher Scientific). The beads were washed 2 × 5 min in ChIP Wash Buffer 1 (0.1% SDS, 1% Triton X-100, 20 mM Tris−HCl pH 8, 2 mM EDTA pH 8, 150 mM NaCl), 2 × 5 min in ChIP Wash Buffer 2 (0.1% SDS, 1% Triton X-100, 20 mM Tris−HCl pH 8, 2 mM EDTA pH 8, 500 mM NaCl), 2 × 5 min in ChIP Wash Buffer 3 (0.25 mM LiCl, 1% NP-40, 1% sodium deoxycholate, 10 mM Tris−HCl pH 8, 1 mM EDTA pH 8) and twice in TE (10 mm Tris-HCl pH 8, 1 mM EDTA pH 8). ChIPed DNA was eluted by two 15-min incubations at 65°C with 250 µl of Elution Buffer (1% SDS, 0.1 m NaHCO3). Chromatin was reverse-cross-linked by adding 20 µl of NaCl 5 M and incubated overnight at 65°C. Reverse cross-linked DNA was submitted to RNase and Proteinase K treatment, and extracted with phenol−chloroform. DNA was ethanol precipitated in the presence of 20 µg of glycogen and resuspended in 10 µl of nuclease-free water in a DNA low-bind tube. Libraries were then generated using 10ng of DNA and NEBNext Ultra II DNA Library Prep Kit for Illumina (NEB). The quality of the libraries was assessed with Agilent 2100 Bioanalyzer (Agilent), and the libraries were subjected to 1 × 75 bp high-throughput sequencing by NextSeq 500 (Illumina).

HiChIP assay

HiChIP experiments were performed on shoots and roots of 14-day-old-seedlings using the same procedure as in Concia et al (Concia et al. 2020) with either anti-H3K9ac (Millipore 07–352) or anti-H3K27me3 (Millipore 07–449). The quality of the libraries was assessed with Agilent 2100 Bioanalyzer

(Agilent), and the libraries were subjected to 2 × 75 bp paired-end high-throughput sequencing by NextSeq 500 (Illumina).

Capture Hi-C assay

For capture Hi-C, in situ Hi-C libraries from shoot and root of Col-0, *ref6*, and *clf* were first generated as in Concia et al (Concia et al. 2020). The quality and the DNA concentration of the libraries were assessed with Agilent 2100 Bioanalyzer (Agilent). Capture was then performed using SureSelect XT Target Enrichment System for Illumina Paired-End Multiplexed Sequencing Library (Agilent) according to manufacturer's recommendation. To this end, 52911 custom probes were designed, covering 2.658 Mbp and 4650 genes (Supplemental Table S25). Capture was performed using 1µg of in situ Hi-C libraries and following manufacturer's recommendation. Quality control and sequencing of the libraries were done in the same way as for HiChIP assays.

Analysis of ChIP-seq data

Single-end sequencing of ChIP samples was performed using Illumina NextSeq 500 with a read length of 76 bp. Trimmomatic-0.38 (Martin 2011) was used for quality trimming. Parameters for read quality filtering were set as follows: Minimum length of 36 bp; Mean Phred quality score greater than 30; Leading and trailing bases removal with base quality <5. The reads were mapped onto the TAIR10 assembly using Bowtie 2 (Langmead and Salzberg 2012) with mismatch permission of 1 bp. To identify significantly enriched regions, we used MACS2 (Gaspar 2018) Parameters for peaks detection were set as follows: Number of duplicate reads at a location:1; mfold of 5:50; q-value cutoff: 0.05; extsize 200; broad peak. To extract the average scores across the genomic regions, multiBigwigSummary command from the deepTools package (Ramírez et al. 2016) was used with default parameters on the RPGC normalized bigWig files.

Differential expression analysis

Single-end sequencing of RNA-seq samples were trimmed using Trimmomatic-0.38 with the parameters: Minimum length of 30 bp; Mean Phred quality score greater than 30; Leading and trailing bases removal with base quality <5. STAR aligner (Dobin et al. 2013) was used to mapped the reads to TAIR10 genome assembly. Raw read counts were then extracted using featureCounts based on the gene annotations in Araport11_GFF3_genes_transposons.201606.gtf. Finally, we used DESeq2 (Love et al. 2014) to identify differentially expressed genes. Genes having read counts ≥ 50 in atleast 2 samples were considered for differential expression analysis.

Analysis of HiChIP and Capture Hi-C data

Raw FASTQ files were preprocessed with Trimmomatic-0.38 to remove Illumina sequencing adapters. The 5' and 3' ends with a quality score below 5 (Phred+33) were trimmed and reads shorter than 30 bp after trimming were dropped. The trimmed files were then processed with HiC-Pro v2.11.1 (Servant et al. 2015). The reads were aligned using Bowtie 2 onto the TAIR10 assembly with default settings, except for the parameter "--score-min L, -0.6, -0.8". Invalid ligation products (such as dangling ends, fragments ligated on themselves, and ligations of juxtaposed fragments) were discarded. Valid pairs were used to produce raw interaction matrixes at various resolutions. Finally, ".hic" files were generated with the software Juicer Tools and visualized with the tool Juicebox (Durand et al. 2016).

Identification and analysis of genomic interactions

Valid pairs generated are further analysed using HOMER v4.10 (Zhang et al. 2008) for different resolutions (500bp for short range interactions and 20kb for long range interactions). For the short range interactions, both the anchors of the interactions (genomic bins) were annotated with genes using BEDTools intersect. We removed interactions without any gene annotations, self-loops and duplicates.

Finally, based on the gene annotations, we integrated the log fold-change from RNA-seq data and ChIP-seq data.

Data access

All raw and processed sequencing data generated in this study have been submitted to the NCBI Gene Expression Omnibus (GEO; https://www.ncbi.nlm.nih.gov/geo/query/acc.cgi) under accession number GSE155502.

Competing interest statement

The authors declare no competing interests.

Acknowledgments

This work was supported by the Agence National de la Recherche ANR (3DWheat project ANR-19-CE20-0001-01) and by the Institut Universitaire de France (IUF).

Y.H. was supported by China Scholar Council fellowships (201806690005).

Author contributions

M.B. designed this research project. Y.H., J.R. N.R.G. and R.B. collected the plant materials. Y.H. and D.L. performed the Capture Hi-C, HiChIP, ChIP-seq experiments and Capture Hi-C, HiChIP, ChIP-seq libraries. D.L. performed the Illumina sequencing and Immunofluorescence staining experiments. S.S., J.R, D.M, J.A., D.L, L.C. and M.B. performed the bioinformatics analyses. Y.H., S.S., D.L. and M.B. made figures and supplement data. M.B. F.A and J.R wrote the paper with support from all authors. M.M, S.A, A.V.P, F.B, C.B., F.A, H.H., M.C., J.G.M., C.R., D.L analyzed the data and provided critical feedback. The authors read and approved the final manuscript.

562 **References**

563 Ahmad A, Zhang Y, Cao X. 2010. Decoding the Epigenetic Language of Plant Development. *Mol Plant* **3**:
564 719–728.

565 Antunez-Sanchez J, Naish M, Ramirez-Prado JS, Ohno S, Huang Y, Dawson A, Opassathian K, Manza-
566 Mianza D, Ariel F, Raynaud C, et al. 2020. A new role for histone demethylases in the maintenance
567 of plant genome integrity. *Elife* **9**: 1–32.

568 Bantignies F, Roure V, Comet I, Leblanc B, Schuettengruber B, Bonnet J, Tixier V, Mas A, Cavalli G. 2011.
569 Polycomb-dependent regulatory contacts between distant hox loci in drosophila. *Cell* **144**: 214–226.

570 Berry S, Rosa S, Howard M, Bühler M, Dean C. 2017. Disruption of an RNA-binding hinge region abolishes
571 LHP1-mediated epigenetic repression. *Genes Dev* **31**: 2115–2120.

572 Boettiger AN, Bintu B, Moffitt JR, Wang S, Beliveau BJ, Fudenberg G, Imakaev M, Mirny LA, Wu CT,
573 Zhuang X. 2016. Super-resolution imaging reveals distinct chromatin folding for different epigenetic
574 states. *Nature* **529**: 418–422.

575 Cheng K, Xu Y, Yang C, Ouellette L, Niu L, Zhou X, Chu L, Zhuang F, Liu J, Wu H, et al. 2020. Histone tales:
576 Lysine methylation, a protagonist in Arabidopsis development. *J Exp Bot* **71**: 793–807.

577 Cheutin T, Cavalli G. 2014. Polycomb silencing: From linear chromatin domains to 3D chromosome
578 folding. *Curr Opin Genet Dev* **25**: 30–37.

579 Choi J, Strickler SR, Richards EJ. 2019. Loss of CRWN nuclear proteins induces cell death and salicylic acid
580 defense signaling. *Plant Physiol* **179**: 1315–1329.

581 Concia L, Veluchamy A, Ramirez-Prado JS, Martin-Ramirez A, Huang Y, Perez M, Domenichini S,
582 Rodriguez-Granados NY, Kim S-K, Blein T, et al. 2020. Wheat chromatin architecture is organized in
583 genome territories and transcription factories. *Genome Biol* **ACCEPTED**.

584 de Wit E, Vos ESM, Holwerda SJB, Valdes-Quezada C, Verstegen MJAM, Teunissen H, Splinter E, Wijchers
585 PJ, Krijger PHL, de Laat W. 2015. CTCF Binding Polarity Determines Chromatin Looping. *Mol Cell* **60**:

676–684.

Dekker J, Heard E. 2015. Structural and functional diversity of Topologically Associating Domains. *FEBS Lett* **589**: 2877–2884.

Dixon JR, Gorkin DU, Ren B. 2016. Chromatin Domains: The Unit of Chromosome Organization. *Mol Cell* **62**: 668–680.

Dixon JR, Selvaraj S, Yue F, Kim A, Li Y, Shen Y, Hu M, Liu JS, Ren B. 2012. Topological domains in mammalian genomes identified by analysis of chromatin interactions. *Nature* **485**: 376–380.

Dobin A, Davis CA, Schlesinger F, Drenkow J, Zaleski C, Jha S, Batut P, Chaisson M, Gingeras TR. 2013. STAR: Ultrafast universal RNA-seq aligner. *Bioinformatics* **29**: 15–21.

Dong P, Tu X, Chu PY, Lü P, Zhu N, Grierson D, Du B, Li P, Zhong S. 2017a. 3D Chromatin Architecture of Large Plant Genomes Determined by Local A/B Compartments. *Mol Plant* **10**: 1497–1509. https://doi.org/10.1016/j.molp.2017.11.005 (Accessed January 2, 2021).

Dong P, Tu X, Chu PY, Lü P, Zhu N, Grierson D, Du B, Li P, Zhong S. 2017b. Comprehensive mapping of long range interactions reveals folding principles of the human genome. *Mol Plant* **10**: 1497–1509.

Dong Q, Li N, Li X, Yuan Z, Xie D, Wang X, Li J, Yu Y, Wang J, Ding B, et al. 2018. Genome-wide Hi-C analysis reveals extensive hierarchical chromatin interactions in rice. *Plant J* **94**: 1141–1156.

Du Z, Zheng H, Kawamura YK, Zhang K, Gassler J, Powell S, Xu Q, Lin Z, Xu K, Zhou Q, et al. 2020. Polycomb Group Proteins Regulate Chromatin Architecture in Mouse Oocytes and Early Embryos. *Mol Cell* **77**: 825-839.e7.

Durand NC, Robinson JT, Shamim MS, Machol I, Mesirov JP, Lander ES, Lieberman E, Correspondence A. 2016. Juicebox Provides a Visualization System for Hi-C Contact Maps with Unlimited Zoom. *Cell Syst* **3**: 99–101.

Eichten SR, Schmitz RJ, Springer NM. 2014. Epigenetics: Beyond Chromatin Modifications and Complex Genetic Regulation. *Plant Physiol* **165**: 933–947.

El-Sharnouby S, Fischer B, Magbanua JP, Umans B, Flower R, Choo SW, Russell S, White R. 2017. Regions of very low H3K27me3 partition the Drosophila genome into topological domains. *PLoS One* **12**: 1–23.

Eskeland R, Leeb M, Grimes GR, Kress C, Boyle S, Sproul D, Gilbert N, Fan Y, Skoultchi AI, Wutz A, et al. 2010. Ring1B Compacts Chromatin Structure and Represses Gene Expression Independent of Histone Ubiquitination. *Mol Cell* **38**: 452–464.

Feng S, Cokus SJ, Schubert V, Zhai J, Pellegrini M, Jacobsen SE. 2014. Genome-wide Hi-C Analyses in Wild-Type and Mutants Reveal High-Resolution Chromatin Interactions in Arabidopsis. *Mol Cell* **55**: 694–707. /pmc/articles/PMC4347903/?report=abstract (Accessed January 10, 2021).

Fortin JP, Hansen KD. 2015. Reconstructing A/B compartments as revealed by Hi-C using long-range correlations in epigenetic data. *Genome Biol* **16**: 1–23.

Francis NJ, Kingston RE, Woodcock CL. 2004. Chromatin compaction by a polycomb group protein complex. *Science (80-)* **306**: 1574–1577.

Fullwood MJ, Liu MH, Pan YF, Liu J, Xu H, Mohamed Y Bin, Orlov YL, Velkov S, Ho A, Mei PH, et al. 2009. An oestrogen-receptor-α-bound human chromatin interactome. *Nature* **462**: 58–64.

Gambino G, Pantaleo V. 2017. Epigenetics in plant-pathogen interactions. In *Plant Epigenetics* (ed. J.B. Nikolaus Rajewsky, Stefan Jurga), pp. 385–404, Springer Nature, Cham, Switzerland.

Gaspar J. 2018. Improved peak-calling with MACS2. *bioRxiv* 496521.

Gaudin V, Libault M, Pouteau S, Juul T, Zhao G, Lefebvre D, Grandjean O. 2001. Mutations in LIKE HETEROCHROMATIN PROTEIN 1 affect flowering time and plant architecture in Arabidopsis. *Development* **128**: 4847–58.

Gonzalez-Sandoval A, Gasser SM. 2016. On TADs and LADs: Spatial Control Over Gene Expression. *Trends Genet* **32**: 485–495.

Grob S, Schmid MW, Grossniklaus U. 2014. Hi-C Analysis in Arabidopsis Identifies the KNOT, a Structure

with Similarities to the flamenco Locus of Drosophila. *Mol Cell* **55**: 678–693.

Grossniklaus U, Paro R. 2014. Transcriptional Silencing by Polycomb Group proteins. *Cold Spring Harb Perspect Biol* **6**: 1–20.

Guo Y, Xu Q, Canzio D, Shou J, Li J, Gorkin DU, Jung I, Wu H, Zhai Y, Tang Y, et al. 2015. CRISPR Inversion of CTCF Sites Alters Genome Topology and Enhancer/Promoter Function. *Cell* **162**: 900–910.

Ha M, Ng DW, Li W, Chen ZJ. 2011. Coordinated histone modifications are associated with gene expression variation within and between species. 590–598.

Hernández-Muñoz I, Taghavi P, Kuijl C, Neefjes J, van Lohuizen M. 2005. Association of BMI1 with Polycomb Bodies Is Dynamic and Requires PRC2/EZH2 and the Maintenance DNA Methyltransferase DNMT1. *Mol Cell Biol* **25**: 11047–11058.

Hou X, Zhou J, Liu C, Liu L, Shen L, Yu H. 2014. Nuclear factor Y-mediated H3K27me3 demethylation of the SOC1 locus orchestrates flowering responses of Arabidopsis. *Nat Commun* **5**: 1–14.

Hu B, Wang N, Bi X, Karaaslan ES, Weber AL, Zhu W, Berendzen KW, Liu C. 2019. Plant lamin-like proteins mediate chromatin tethering at the nuclear periphery. *Genome Biol* **20**: 1–18.

Huang Y, Rodriguez-Granados NY, Latrasse D, Raynaud C, Benhamed M, Ramirez-Prado JS. 2020. The matrix revolutions: towards the decoding of the plant chromatin three-dimensional reality. *J Exp Bot* **71**: 5129–5147.

Illingworth RS. 2019. Chromatin folding and nuclear architecture: PRC1 function in 3D. *Curr Opin Genet Dev* **55**: 82–90.

Joshi O, Wang SY, Kuznetsova T, Atlasi Y, Peng T, Fabre PJ, Habibi E, Shaik J, Saeed S, Handoko L, et al. 2015. Dynamic Reorganization of Extremely Long-Range Promoter-Promoter Interactions between Two States of Pluripotency. *Cell Stem Cell* **17**: 748–757.

Kaiser VB, Semple CA. 2017. When TADs go bad: chromatin structure and nuclear organisation in human disease. *F1000Research* **6**: 314.

Kassis JA, Kennison JA, Tamkun JW. 2017. Polycomb and trithorax group genes in drosophila. *Genetics* **206**: 1699–1725.

Kouzarides T. 2007. Chromatin Modifications and Their Function. *Cell* **128**: 693–705.

Kundu S, Ji F, Sunwoo H, Jain G, Lee JT, Sadreyev RI, Dekker J, Kingston RE. 2017. Polycomb Repressive Complex 1 Generates Discrete Compacted Domains that Change during Differentiation. *Mol Cell* **65**: 432-446.e5.

Langmead B, Salzberg SL. 2012. Fast gapped-read alignment with Bowtie 2. *Nat Methods* **9**: 357–359.

Lanzuolo C, Roure V, Dekker J, Bantignies F, Orlando V. 2007. Polycomb response elements mediate the formation of chromosome higher-order structures in the bithorax complex. **9**.

Latrasse D, Jégu T, Li H, de Zelicourt A, Raynaud C, Legras S, Gust A, Samajova O, Veluchamy A, Rayapuram N, et al. 2017. MAPK-triggered chromatin reprogramming by histone deacetylase in plant innate immunity. *Genome Biol* **18**: 1–19.

Lieberman-Aiden E, van Berkum NL, Williams L, Imakaev M, Ragoczy T, Telling A, Amit I, Lajoie BR, Sabo PJ, Dorschner MO, et al. 2009. Comprehensive Mapping of Long-Range Interactions Reveals Folding Principles of the Human Genome. *Science (80-)* **326**: 289–293.

Liu C, Cheng YJ, Wang JW, Weigel D. 2017. Prominent topologically associated domains differentiate global chromatin packing in rice from Arabidopsis. *Nat Plants* **3**: 742–748.

Liu C, Wang C, Wang G, Becker C, Weigel D. 2016a. Genome-wide analysis of chromatin packing in Arabidopsis thaliana at single- gene resolution. *Genome Res* 1–30.

Liu J, Deng S, Wang H, Ye J, Wu HW, Sun HX, Chua NH. 2016b. CURLY LEAF regulates gene sets coordinating seed size and lipid biosynthesis. *Plant Physiol* **171**: 424–436.

Love MI, Huber W, Anders S. 2014. Moderated estimation of fold change and dispersion for RNA-seq data with DESeq2. *Genome Biol* **15**: 550.

Lu F, Cui X, Zhang S, Jenuwein T, Cao X. 2011. Arabidopsis REF6 is a histone H3 lysine 27 demethylase.

682 *Nat Genet* **43**: 715–719.
683 Lupiáñez DG, Kraft K, Heinrich V, Krawitz P, Brancati F, Klopocki E, Horn D, Kayserili H, Opitz JM, Laxova R,
684 et al. 2015. Disruptions of Topological Chromatin Domains Cause Pathogenic Rewiring of Gene-
685 Enhancer Interactions. *Cell* **161**: 1012–1025.
686 Lupiáñez DG, Spielmann M, Mundlos S. 2016. Breaking TADs: How Alterations of Chromatin Domains
687 Result in Disease. *Trends Genet* **32**: 225–237.
688 Mach J. 2018. In the Histone Zone: The Mighty Eraser. *Plant Cell* **30**: 5–6.
689 Martin M. 2011. Cutadapt removes adapter sequences from high-throughput sequencing reads.
690 *EMBnet.journal* **17**: 10.
691 Mascher M, Gundlach H, Himmelbach A, Beier S, Twardziok SO, Wicker T, Radchuk V, Dockter C, Hedley
692 PE, Russell J, et al. 2017. A chromosome conformation capture ordered sequence of the barley
693 genome. *Nature* **544**: 427.
694 McLaughlin K, Flyamer IM, Thomson JP, Mjoseng HK, Shukla R, Williamson I, Grimes GR, Illingworth RS,
695 Adams IR, Pennings S, et al. 2019. DNA Methylation Directs Polycomb-Dependent 3D Genome Re-
696 organization in Naive Pluripotency. *Cell Rep* **29**: 1974-1985.e6.
697 Melé M, Rinn JL. 2016. "Cat's Cradling" the 3D Genome by the Act of LncRNA Transcription. *Mol Cell* **62**:
698 657–664.
699 Mifsud B, Tavares-Cadete F, Young AN, Sugar R, Schoenfelder S, Ferreira L, Wingett SW, Andrews S, Grey
700 W, Ewels PA, et al. 2015. Mapping long-range promoter contacts in human cells with high-
701 resolution capture Hi-C. *Nat Genet* **47**: 598–606.
702 Mirouze M, Lieberman-Lazarovich M, Aversano R, Bucher E, Nicolet J, Reinders J, Paszkowski J. 2012.
703 Loss of DNA methylation affects the recombination landscape in Arabidopsis. *Proc Natl Acad Sci U S*
704 *A* **109**: 5880–5885. www.pnas.org/lookup/suppl/doi:10.1073/pnas.1120841109/-
705 /DCSupplemental.5880-5885%7CPNAS%7Cwww.pnas.org/cgi/doi/10.1073/pnas.1120841109

(Accessed February 13, 2021).

Mishra A, Hawkins RD. 2017. Three-dimensional genome architecture and emerging technologies: looping in disease. *Genome Med* **9**: 87.

Misteli T. 2007. Beyond the Sequence: Cellular Organization of Genome Function. *Cell* **128**: 787–800.

Mozgova I, Köhler C, Hennig L. 2015. Keeping the gate closed: functions of the polycomb repressive complex PRC2 in development. *Plant J* **83**: 121–132.

Mumbach MR, Rubin AJ, Flynn RA, Dai C, Khavari PA, Greenleaf WJ, Chang HY. 2016. HiChIP: Efficient and sensitive analysis of protein-directed genome architecture. *Nat Methods* **13**: 919–922. https://www.nature.com/articles/nmeth.3999 (Accessed April 22, 2021).

Noh B, Lee SS-H, Kim HH-J, Yi G, Shin E-AEA, Lee M, Jung K-JK, Doyle MMR, Amasino RMR, Noh Y-SY. 2004. Divergent Roles of a Pair of Homologous Jumonji/Zinc-Finger-Class Transcription Factor Proteins in the Regulation of Arabidopsis Flowering Time. *Plant Cell* **16**: 2601–2613.

Nützmann H-W, Doerr D, Ramírez-Colmenero A, Sotelo-Fonseca JE, Wegel E, Stefano M Di, Wingett SW, Fraser P, Hurst L, Fernandez-Valverde SL, et al. 2020. Active and repressed biosynthetic gene clusters have spatially distinct chromosome states. *Proc Natl Acad Sci* **117**: 13800–13809.

Ogiyama Y, Schuettengruber B, Papadopoulos GL, Chang JM, Cavalli G. 2018. Polycomb-Dependent Chromatin Looping Contributes to Gene Silencing during Drosophila Development. *Mol Cell* **71**: 73-88.e5. https://doi.org/10.1016/j.molcel.2018.05.032 (Accessed February 1, 2021).

Pachano T, Crispatzu G, Rada-Iglesias A. 2019. Polycomb proteins as organizers of 3D genome architecture in embryonic stem cells. *Brief Funct Genomics* **18**: 358–366.

Pfluger J, Wagner D. 2007. Histone modifications and dynamic regulation of genome accessibility in plants. *Curr Opin Plant Biol* **10**: 645–652.

Ramírez F, Ryan DP, Grüning B, Bhardwaj V, Kilpert F, Richter AS, Heyne S, Dündar F, Manke T. 2016. deepTools2: a next generation web server for deep-sequencing data analysis. *Nucleic Acids Res* **44**:

W160–W165.

Rao SSP, Huang S-C, Glenn B, Hilaire S, Casellas R, Lander ES, Lieberman E, Correspondence A. 2017. Cohesin Loss Eliminates All Loop Domains. *Cell* **171**: 305-309.e24. https://doi.org/10.1016/j.cell.2017.09.026 (Accessed February 1, 2021).

Ricci WA, Lu Z, Ji L, Marand AP, Ethridge CL, Murphy NG, Noshay JM, Galli M, Mejía-Guerra MK, Colomé-Tatché M, et al. 2019. Widespread long-range cis-regulatory elements in the maize genome. *Nat Plants* **5**: 1237–1249.

Rocha PP, Raviram R, Bonneau R, Skok JA. 2015. Breaking TADs: Insights into hierarchical genome organization. *Epigenomics* **7**: 523–526.

Rodriguez-Granados NY, Ramirez-Prado JS, Veluchamy A, Latrasse D, Raynaud C, Crespi M, Ariel F, Benhamed M. 2016. Put your 3D glasses on: plant chromatin is on show. *J Exp Bot* **67**: 1–17.

Rosa-Garrido M, Chapski DJ, Schmitt AD, Kimball TH, Karbassi E, Monte E, Balderas E, Pellegrini M, Shih T-T, Soehalim E, et al. 2017. High-Resolution Mapping of Chromatin Conformation in Cardiac Myocytes Reveals Structural Remodeling of the Epigenome in Heart Failure. *Circulation* **136**: 1613–1625.

Rosencrance CD, Ammouri HN, Yu Q, Ge T, Rendleman EJ, Marshall SA, Eagen KP. 2020. Chromatin Hyperacetylation Impacts Chromosome Folding by Forming a Nuclear Subcompartment. *Mol Cell* **78**: 112-126.e12.

Rowley MJ, Corces VG. 2016. The three-dimensional genome: principles and roles of long-distance interactions. *Curr Opin Cell Biol* **40**: 8–14.

Rowley MJ, Nichols MH, Lyu X, Ando-Kuri M, Rivera ISM, Hermetz K, Wang P, Ruan Y, Corces VG. 2017. Evolutionarily Conserved Principles Predict 3D Chromatin Organization. *Mol Cell* **67**: 837-852.e7.

Schoenfelder S, Sugar R, Dimond A, Javierre BM, Armstrong H, Mifsud B, Dimitrova E, Matheson L, Tavares-Cadete F, Furlan-Magaril M, et al. 2015. Polycomb repressive complex PRC1 spatially

constrains the mouse embryonic stem cell genome. *Nat Genet* **47**: 1179–1186.

Servant N, Varoquaux N, Lajoie BR, Viara E, Chen CJ, Vert JP, Heard E, Dekker J, Barillot E. 2015. HiC-Pro: An optimized and flexible pipeline for Hi-C data processing. *Genome Biol* **16**: 259.

Sutherland H, Bickmore WA. 2009. Transcription factories: gene expression in unions? *Nat Rev Genet* **10**: 457–466.

Turck F, Roudier F, Farrona S, Martin-Magniette M-LL, Guillaume E, Buisine N, Gagnot S, Martienssen RA, Coupland G, Colot V. 2007. Arabidopsis TFL2/LHP1 Specifically Associates with Genes Marked by Trimethylation of Histone H3 Lysine 27. *PLoS Genet* **3**: 0855–0866.

Veluchamy A, Jégu T, Ariel F, Latrasse D, Mariappan KG, Kim S-KK, Crespi M, Hirt H, Bergounioux C, Raynaud C, et al. 2016. LHP1 Regulates H3K27me3 Spreading and Shapes the Three-Dimensional Conformation of the Arabidopsis Genome ed. M. Bendahmane. *PLoS One* **11**: e0158936.

Wang C, Liu C, Roqueiro D, Grimm D, Schwab R, Becker C, Lanz C, Weigel D. 2015. Genome-wide analysis of local chromatin packing in Arabidopsis thaliana. *Genome Res* **25**: 246–256.

Wang M, Wang P, Lin M, Ye Z, Li G, Tu L, Shen C, Li J, Yang Q, Zhang X. 2018. Evolutionary dynamics of 3D genome architecture following polyploidization in cotton. *Nat Plants* **4**: 90–97.

Williamson I, Eskeland R, Lettice LA, Hill AE, Boyle S, Grimes GR, Hill RE, Bickmore WA. 2012. Anterior-posterior differences in HoxD chromatin topology in limb development. *Dev* **139**: 3157–3167.

Yan W, Chen D, Smaczniak C, Engelhorn J, Liu H, Yang W, Graf A, Carles CC, Zhou D-X, Kaufmann K. 2018. Dynamic and spatial restriction of Polycomb activity by plant histone demethylases. *Nat Plants* **4**: 681–689.

Yun M, Wu J, Workman JL, Li B. 2011. Readers of histone modifications. *Cell Res* **21**: 564–578.

Zhang X, Germann S, Blus BJ, Khorasanizadeh S, Gaudin V, Jacobsen SE. 2007. The Arabidopsis LHP1 protein colocalizes with histone H3 Lys27 trimethylation. *Nat Struct Mol Biol* **14**: 869–71.

Zhang Y, Liu T, Meyer CA, Eeckhoute J, Johnson DS, Bernstein BE, Nussbaum C, Myers RM, Brown M, Li

W, et al. 2008. Model-based analysis of ChIP-Seq (MACS). *Genome Biol* **9**: R137.

Zheng H, Xie W. 2019. The role of 3D genome organization in development and cell differentiation. *Nat Rev Mol Cell Biol* **20**: 535–550.

Zhou S, Jiang W, Zhao Y, Zhou DX. 2019. Single-cell three-dimensional genome structures of rice gametes and unicellular zygotes. *Nat Plants* **5**: 795–800.

Figure legends

Figure 1. *Arabidopsis* chromatin organization displays a strong compartmentalization

(A) Immunofluorescence detection of H3K9ac (green) and H3K27me3 (red) histone histone modifications and DAPI staining (grey) in an isolated *Arabidopsis* nucleus. Scale bar = 5 µm. **(B)** Distribution of immunofluorescence signal intensity in the nucleus. The analysis was performed along the white line shown in the merged image in A. **(C)** Visualization of the interaction matrix of Hi-C and HiChIP in a specific region of the Chromosome 2. H3K9ac ChIP-seq signal (blue peaks) were aligned with the maps to highlight the correlation with HiChIP enriched regions as expected. **(D)** Visualization of the interaction matrix of Hi-C and HiChIP in a specific region of the Chromosome 4. H3K27me3 ChIP-seq signal (red peaks) were aligned with the maps to highlight the correlation with HiChIP enriched regions as expected. **(E)** Visualization of the interaction matrix of HiChIP data of H3K9ac and H3K27me3 in a specific region of the Chromosome 2. Dots showing higher (blue) and lower (red) signals in H3K9ac HiChIP compared to H3K27me3 respectively. ChIP-seq signals of H3K9ac (blue peaks) and H3K27me3 (red peaks) were aligned with the map to highlight the correlation with HiChIP enriched regions.

Figure 2. Shoot and root nuclei display distinct 3D chromatin architecture

(A) Heatmap showing the H3K27me3 HiChIP signal of the top shoot-specific repressive loops (SSRLs). **(B)** Example of long distance SSRL on Chromosome 5. ChIP-seq signals of H3K27me3 in shoot (red peaks) and

802 root (blue peaks) were aligned with the map and the differential analysis of both ChIP-seq signals in
803 differentially interacting regions are highlighted (bottom panels in grey). **(C)** Example of short distance
804 SSRL. H3K27me3 ChIP-seq signal is represented by red peaks and chromatin interactions signal by blue
805 lines. **(D)** Analysis of H3K27me3 levels on SSRLs. The pie chart represents the percentage of the genes
806 involved in SSRLs that are either hyper-methylated in shoot or in root. The boxplot shows the H3K27me3
807 levels in shoot or root of the 47% of shoot hyper-methylated genes involved in SSRLs. **(E)** Scatterplot of
808 $\log_2$ (shoot/root gene expression fold change) for pairs of genes interacting through H3K27me3-
809 associated contacts in shoot. **(F)** Gene Ontology enrichment analysis of the differentially expressed genes
810 involved in SSRLs. **(G)** Heatmap of H3K27me3 HiChIP signal of the top root specific repressive loops
811 (RSRLs). **(H)** Example of long distance RSRLs on Chromosome 1. ChIP-seq signals of H3K27me3 in shoot
812 (red peaks) and root (blue peaks) were aligned with the map and the differential analysis of both ChIP-
813 seq signals in differentially interacting regions are highlighted (bottom panels in grey). **(I)** Example of
814 short distance RSRLs. **(J)** Analysis of H3K27me3 level over RSRLs. The pie chart represents the percentage
815 of genes involved in RSRLs that are either hyper-methylated in shoot or root. The boxplot displayed the
816 H3K27me3 levels of the 48% of root hyper-methylated genes involved in RSRLs. **(K)** Scatterplot of $\log_2$
817 (shoot/root gene expression fold change) for pairs of genes interacting through H3K27me3-associated
818 contacts in root. **(L)** Gene Ontology enrichment analysis of the differentially expressed genes involved in
819 RSRLs.
820
821 **Figure 3. The levels of H3K27me3 correlate with the stability of repressive loops**
822 **(A)** Visualization of the interaction matrix of Hi-C and C-Hi-C in a specific region of the Chromosome 1.
823 **(B)** Example of interaction analysis using C-Hi-C data showing captured regions (green bars), H3K27me3
824 ChIP-seq signal (red peaks) and chromatin interactions (purple lines). **(C)** Heatmap of C-Hi-C data
825 showing the shoot specific loops (SSLs). **(D)** Examples of shoot specific interacting region detected by

both C-Hi-C and H3K27me3 HiChIP. Probes used for the C-Hi-C are represented by green bars, the H3K27me3 ChIP-seq signal by red peaks, the C-Hi-C interaction signals by purple lines and H3K27me3 HiChIP interaction signals by blue lines. **(E)** Venn diagram representing overlap of loops called from HiChIP and C-Hi-C library sets. Only loops containing specific probes were selected for the comparison in HiChIP. **(F)** Pie chart representing the proportion of genes involved in shoot-specific loops that are repressed in shoot (blue, 67%), repressed genes in root (red, 24%) and unchanged (grey, 9%) among the genes involved in loops detected both with HiChIP and C-Hi-C. **(G)** Heatmap of C-Hi-C data showing the top root specific loops (RSLs). **(H)** Examples of root specific interacting region detected by both C-Hi-C and H3K27me3 HiChIP. Probes used for the C-Hi-C are represented by green bars, the H3K27me3 ChIP-seq signal by red peaks, the C-Hi-C interaction signals by purple lines and H3K27me3 HiChIP interaction signals by blue lines. **(I)** Venn diagram representing overlap of loops called from HiChIP and C-Hi-C library sets. Only loops containing specific probes were selected for the comparison in HiChIP. **(J)** Pie chart representing of genes involved in root-specific loops that are repressed in shoot (blue, 35%), repressed genes in root (red, 54%) and unchanged (grey, 11%) among the genes involved in loops detected both with HiChIP and C-Hi-C.

Figure 4. Ectopic deposition of H3K27me3 leads to formation of new chromatin repressive loops

(A) Schema illustrating the antagonistic role of the PRC2 complex (involving the histone methyltransferase CLF) and the histone demethylase REF6 to control H3K27me3 homeostasis and chromatin remodelling. **(B)** Heatmap of Capture Hi-C (C-Hi-C) data showing *ref6-5* specific loops (reSLs). **(C)** Examples of reSLs detected by C-Hi-C. C-Hi-C interaction signal (blue lines) and H3K27me3 ChIP-seq signal in wild-type (black peaks) and *ref6-5* (red peaks) are represented. **(D)** Model of chromatin contacts organization in wild-type and *ref6-5* mutant. **(E)** Histogram representing the percentage of genes (observed O or expected E) involved in reSLs that are either hyper- or hypo- methylated in *ref6-5*

compare to WT. To obtain the expected proportion, we shuffled the H3K27me3 signals 1000 times to obtain the randomized gene counts. The mean of the 1000 permutations was used to determine the expected proportions. The bottom pie chart represents the percentage of *ref6-5* hyper-methylated genes involved in reSLs. The boxplot displays the H3K27me3 levels of the 40% of *ref6-5* hyper-methylated genes involved on reSLs. **(F)** Scatterplot of $\log_2$ (*ref6-5*/wild-type gene expression fold change) for pairs of genes interacting specifically in *ref6-5* compared to wild-type.

Figure 5. Reduction of H3K27me3 levels induces a reconfiguration of chromatin architecture

(A) Heatmap of Capture Hi-C (C-Hi-C) data showing loops that are weaker in *clf* mutant than in wild-type. **(B)** Example of C-Hi-C interactions displaying disrupted loops in *clf* compared to wild-type. C-Hi-C interactions (blue lines) and H3K27me3 ChIP-seq signal in wild-type (red peaks) and *clf* (purple peaks) are represented. **(C)** Histogram representing the percentage of genes (Observed O or Expected E) involved in cSDLs that are either hyper- or hypo- methylated in *clf* compared to WT. To obtain the expected proportion, we shuffled the H3K27me3 signals 1000 times to obtain the randomized gene counts. The mean of the 1000 permutations was used to determine the expected proportions. **(D)** The boxplot displays the H3K27me3 levels of the 40% of *clf* hypo-methylated genes involved in cSDLs. **(E)** The pie chart represents the percentage of *clf* hypo-methylated genes involved in cSDLs . **(F)** Model of chromatin contacts organization in wild-type and *clf* mutant. **(G)** Scatterplot of $\log_2$ (*clf*/wild-type gene expression fold change) for pairs of genes interacting specifically in wild-type compared to *clf*. **(H)** Heatmap presenting the $\log_2$ of odd ratios of combinations of features of interacting genes (see Results). Positive $\log_2$ (odd ratio) indicates enrichment and negative indicates depletion. **(I)** Pie chart representing the proportion of loops involving a gene H3K27me3 hypomethylated and a gene marked or not by H3K9ac in *clf* mutant. Hypo-H3K27me3—No H3K9Ac Loops in *clf* mutant (blue: 40% observed and 61% expected respectively), Hypo-H3K27me3—H3K9Ac Loops (red: 60% observed and 39% expected respectively). **(J)**

Examples of C-Hi-C interactions of a region losing H3K27me3 in *clf* and that tend to establish interactions with regions marked with H3K9ac euchromatin histone modification. C-Hi-C interactions (blue lines), H3K9ac ChIP-seq signal in wild-type and *clf* (green peaks), H3K27me3 ChIP-seq signal in wild-type and *clf* (red peaks) are represented. **(K)** Model of chromatin contacts organization in wild-type and *clf* mutant.

Figure 6. Histone modifiers control chromatin architecture by triggering formation of chromatin repressive or active domains to allow gene co-regulation.

Model of the formation of tissue-specific active and repressive chromatin domains in *Arabidopsis* seedlings. The green structures represent active compartments, which are associated with H3K9ac-marked euchromatin. The pink structures represent PcG-repressive compartments which are associated with H3K27me3-marked facultative heterochromatin.

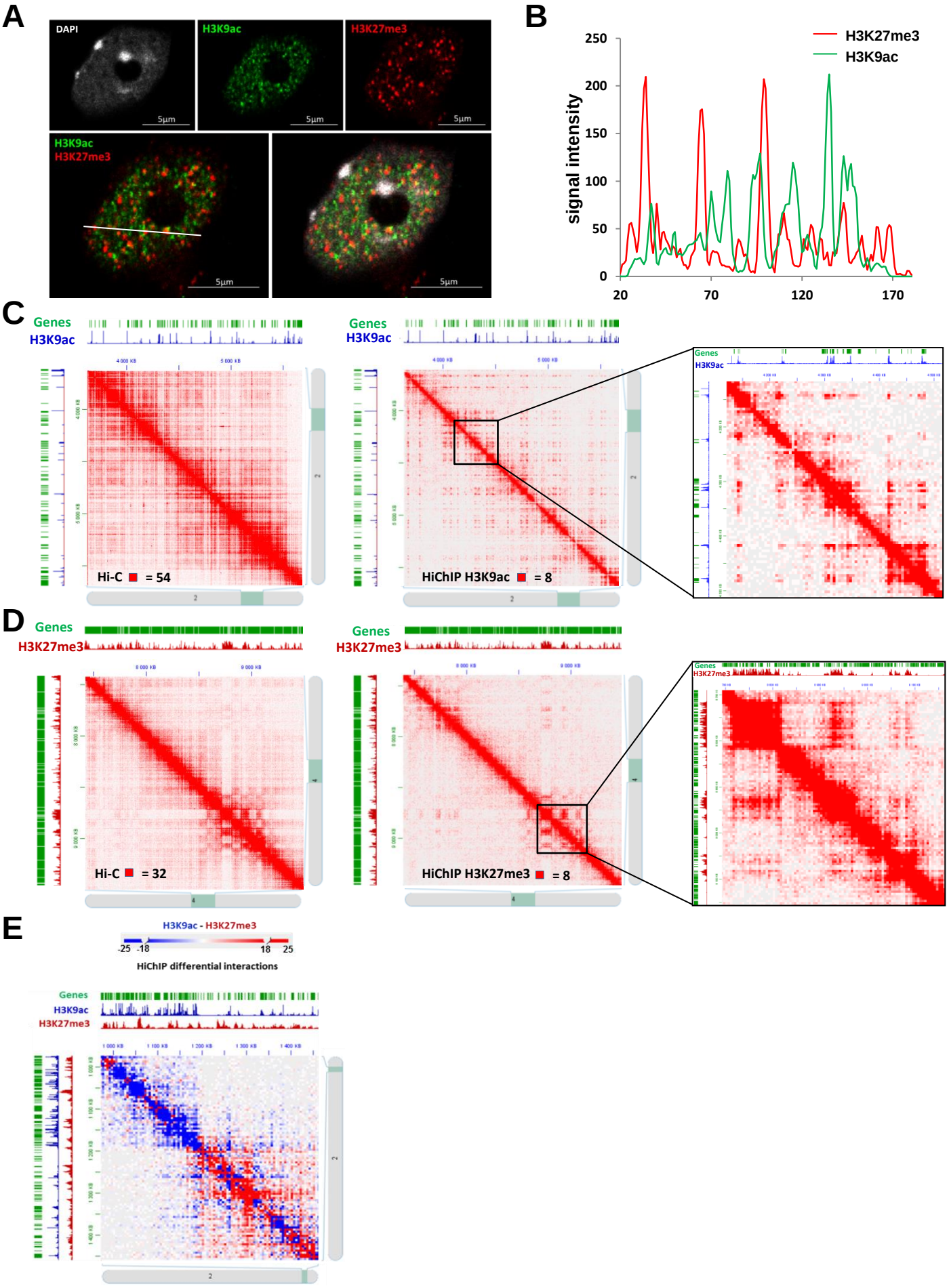
A
DAPI
H3K9ac
H3K27me3
5µm
H3K9ac
H3K27me3
B
H3K27me3
H3K9ac
signal intensity
250
200
150
100
50
0
20
70
120
170
C
Genes
H3K9ac
Hi-C = 54
HiChIP H3K9ac = 8
D
Genes
H3K27me3
Hi-C = 32
HiChIP H3K27me3 = 8
E
H3K9ac - H3K27me3
-25 -18 18 25
HiChIP differential interactions
Genes
H3K9ac
H3K27me3

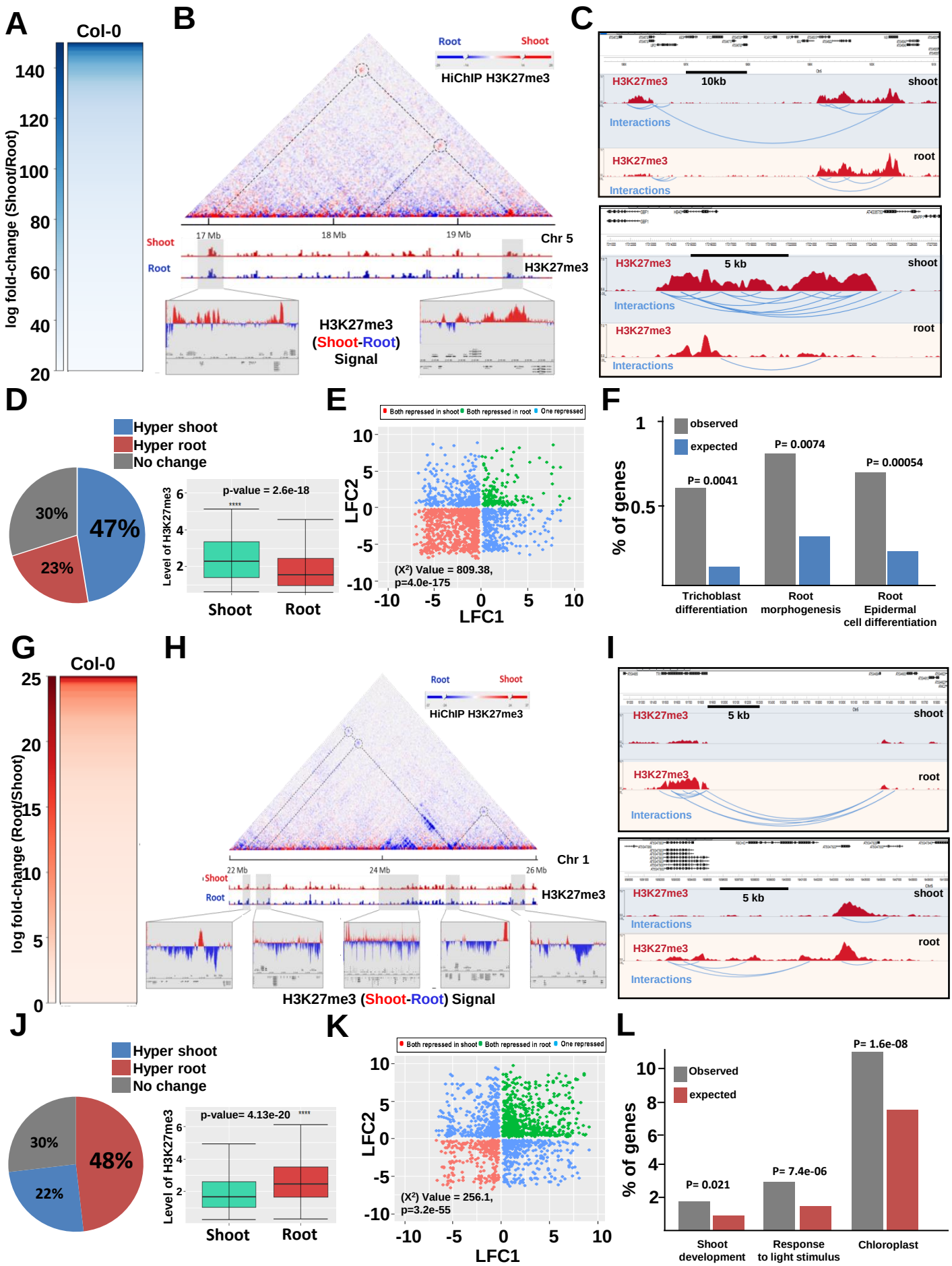
A
Col-0
log fold-change (Shoot/Root)
140
120
100
80
60
40
20
B
Root
Shoot
HiChIP H3K27me3
17 Mb
18 Mb
19 Mb
Chr 5
Shoot
Root
H3K27me3
H3K27me3
(Shoot-Root)
Signal
C
H3K27me3
10kb
shoot
Interactions
H3K27me3
root
Interactions
H3K27me3
5 kb
shoot
Interactions
H3K27me3
root
Interactions
D
Hyper shoot
Hyper root
No change
47%
23%
30%
p-value = 2.6e-18
****
Level of H3K27me3
Shoot
Root
E
Both repressed in shoot
Both repressed in root
One repressed
LFC2
LFC1
(X²) Value = 809.38,
p=4.0e-175
F
observed
expected
% of genes
P= 0.0041
P= 0.0074
P= 0.00054
Trichoblast differentiation
Root morphogenesis
Root Epidermal cell differentiation
G
Col-0
log fold-change (Root/Shoot)
25
20
15
10
5
0
H
Root
Shoot
HiChIP H3K27me3
22 Mb
24 Mb
26 Mb
Chr 1
Shoot
Root
H3K27me3
H3K27me3 (Shoot-Root) Signal
I
H3K27me3
5 kb
shoot
H3K27me3
root
Interactions
H3K27me3
5 kb
shoot
Interactions
H3K27me3
root
Interactions
J
Hyper shoot
Hyper root
No change
48%
22%
30%
p-value= 4.13e-20
****
Level of H3K27me3
Shoot
Root
K
Both repressed in shoot
Both repressed in root
One repressed
LFC2
LFC1
(X²) Value = 256.1,
p=3.2e-55
L
Observed
expected
% of genes
P= 0.021
P= 7.4e-06
P= 1.6e-08
Shoot development
Response to light stimulus
Chloroplast

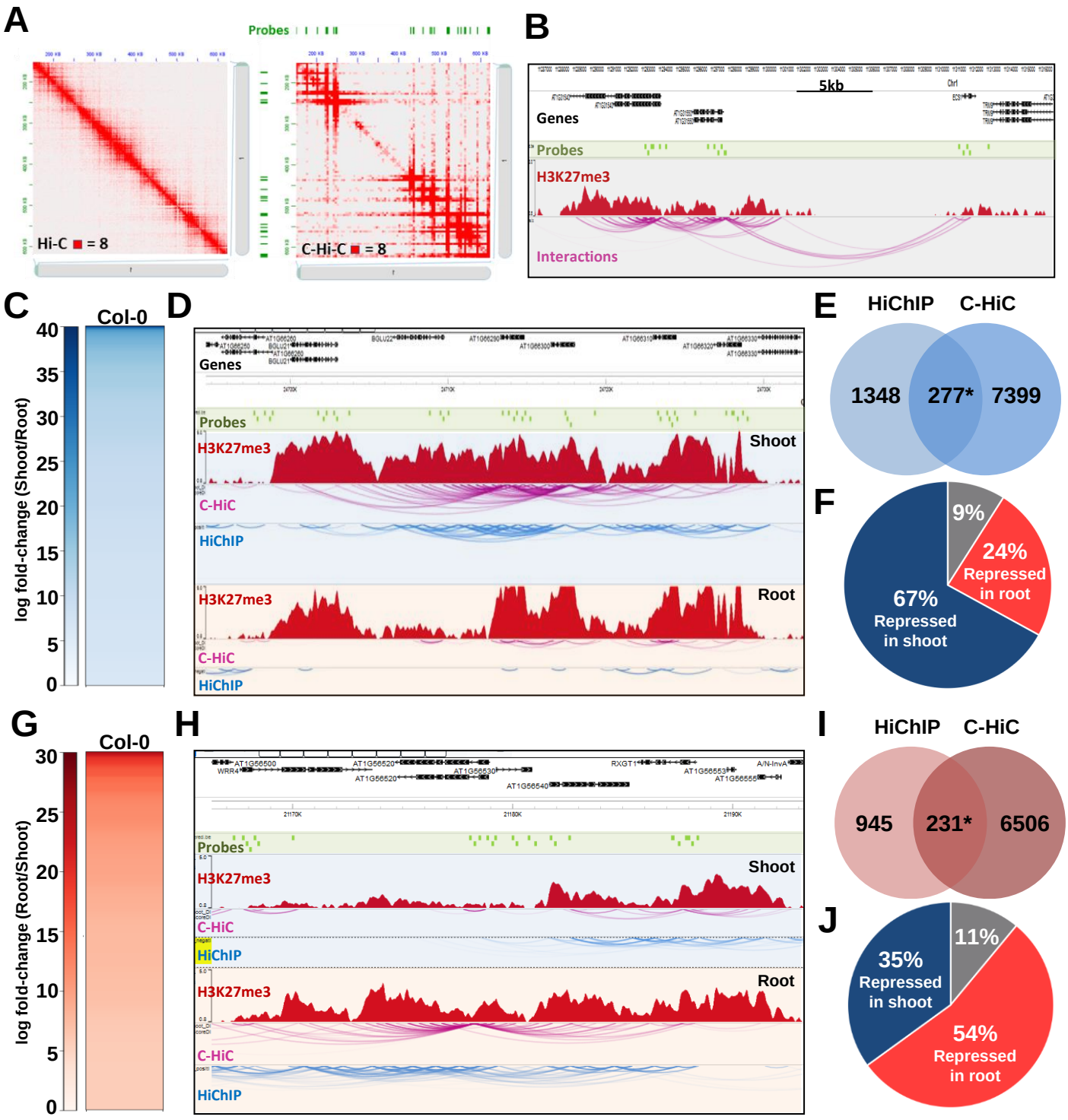
A
Probes
Hi-C ■ = 8
C-Hi-C ■ = 8
B
5kb
Genes
Probes
H3K27me3
Interactions
C
Col-0
log fold-change (Shoot/Root)
40
35
30
25
20
15
10
5
0
D
Genes
Probes
H3K27me3
Shoot
C-HiC
HiChIP
H3K27me3
Root
C-HiC
HiChIP
E
HiChIP
C-HiC
1348
277*
7399
F
9%
24%
Repressed
in root
67%
Repressed
in shoot
G
Col-0
log fold-change (Root/Shoot)
30
25
20
15
10
5
0
H
Probes
H3K27me3
Shoot
C-HiC
HiChIP
H3K27me3
Root
C-HiC
HiChIP
I
HiChIP
C-HiC
945
231*
6506
J
11%
35%
Repressed
in shoot
54%
Repressed
in root

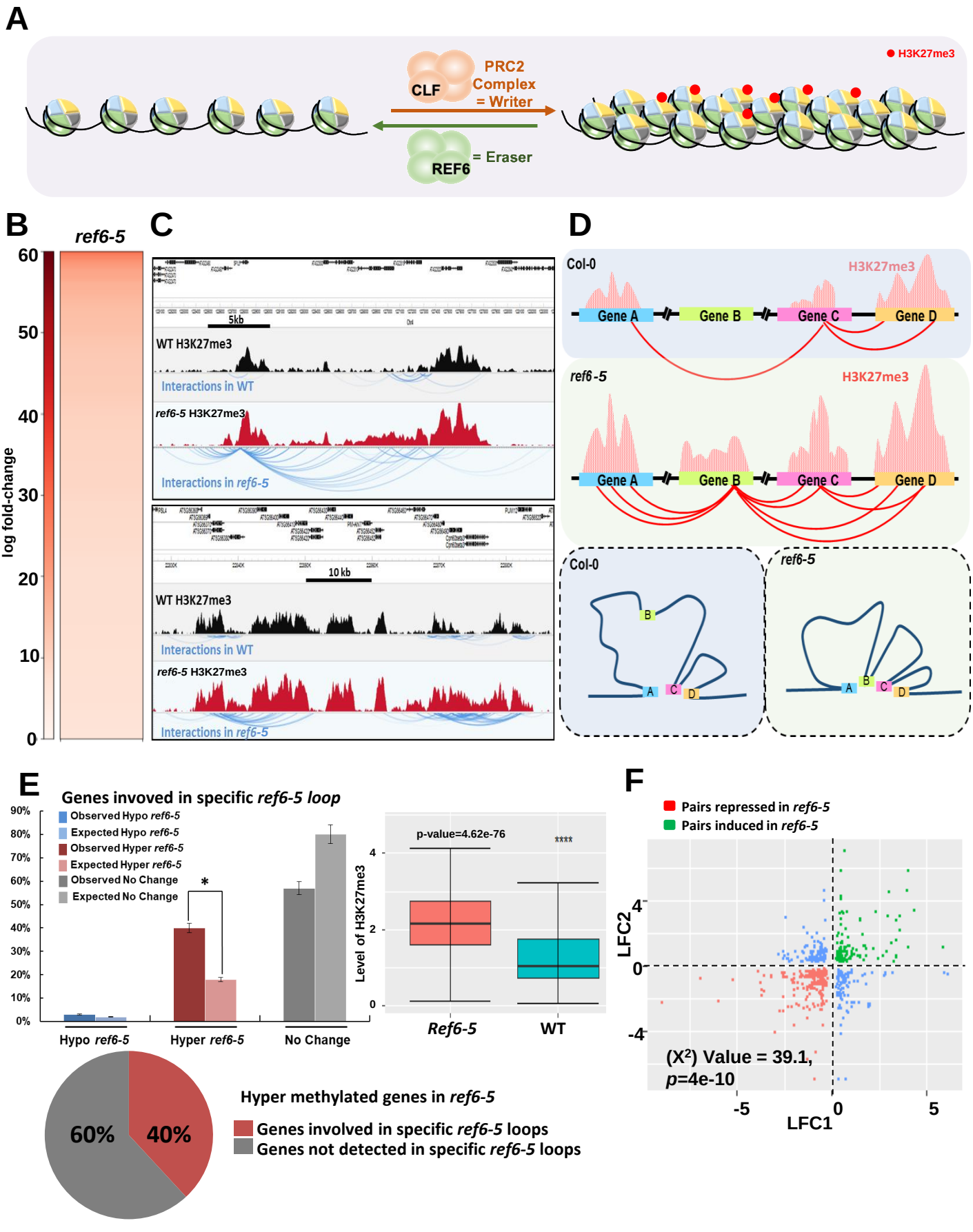
A
H3K27me3
PRC2
Complex
= Writer
CLF
REF6
= Eraser
B
ref6-5
log fold-change
60
50
40
30
20
10
0
C
5kb
WT H3K27me3
Interactions in WT
ref6-5 H3K27me3
Interactions in ref6-5
10 kb
WT H3K27me3
Interactions in WT
ref6-5 H3K27me3
Interactions in ref6-5
D
Col-0
H3K27me3
Gene A
Gene B
Gene C
Gene D
ref6-5
H3K27me3
Gene A
Gene B
Gene C
Gene D
Col-0
ref6-5
E
Genes invoved in specific ref6-5 loop
Observed Hypo ref6-5
Expected Hypo ref6-5
Observed Hyper ref6-5
Expected Hyper ref6-5
Observed No Change
Expected No Change
90%
80%
70%
60%
50%
40%
30%
20%
10%
0%
*
Hypo ref6-5
Hyper ref6-5
No Change
p-value=4.62e-76
****
Level of H3K27me3
4
2
0
Ref6-5
WT
60%
40%
Hyper methylated genes in ref6-5
Genes involved in specific ref6-5 loops
Genes not detected in specific ref6-5 loops
F
Pairs repressed in ref6-5
Pairs induced in ref6-5
LFC2
4
0
-4
(X²) Value = 39.1,
p=4e-10
-5
0
5
LFC1

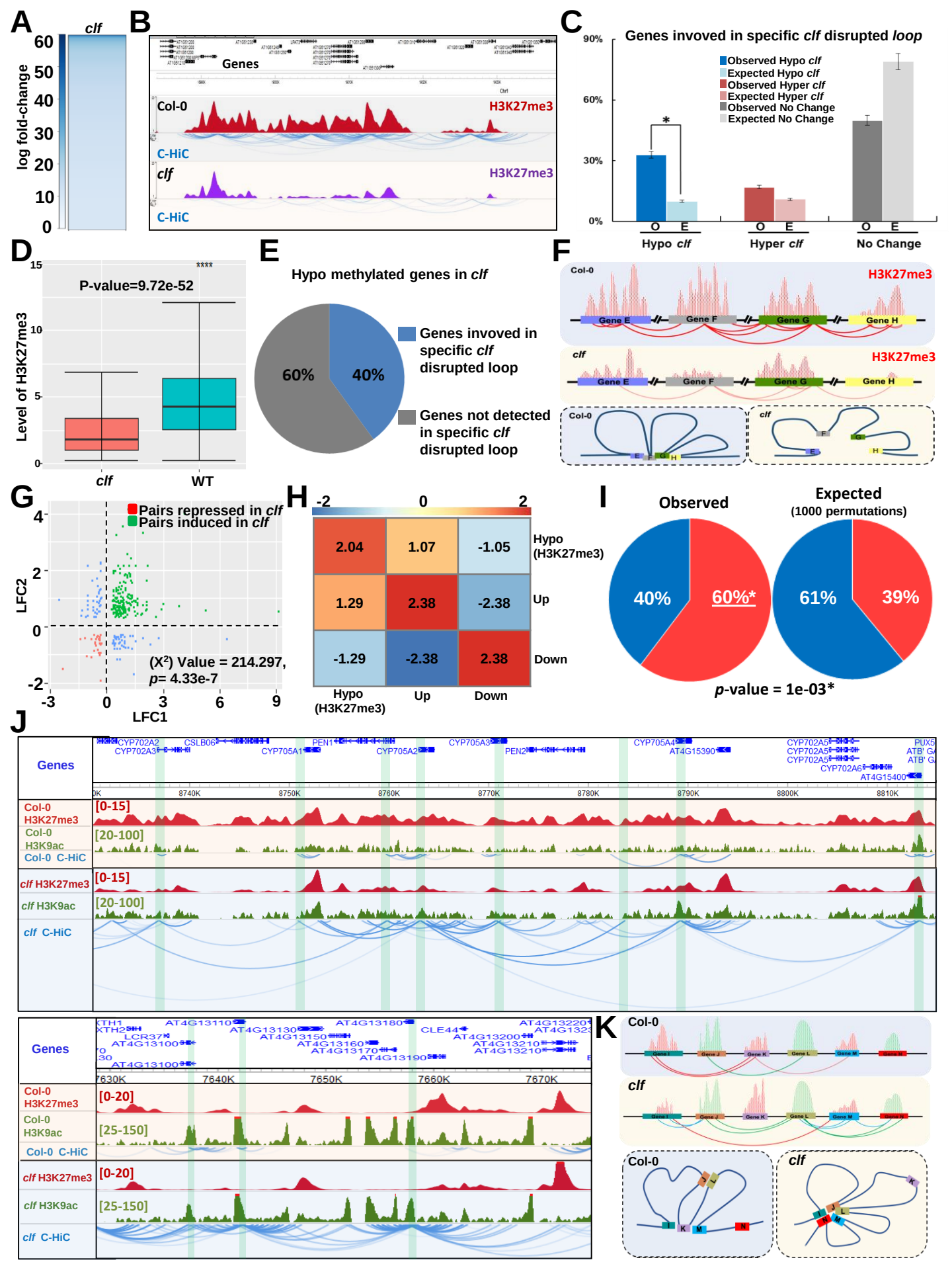
A
clf
log fold-change
60
50
40
30
20
10
0
B
Genes
Col-0
H3K27me3
C-HiC
clf
H3K27me3
C-HiC
C
Genes invoved in specific clf disrupted loop
90%
60%
30%
0%
Observed Hypo clf
Expected Hypo clf
Observed Hyper clf
Expected Hyper clf
Observed No Change
Expected No Change
*
O E
Hypo clf
Hyper clf
No Change
D
P-value=9.72e-52
****
Level of H3K27me3
15
10
5
0
clf
WT
E
Hypo methylated genes in clf
60%
40%
Genes invoved in specific clf disrupted loop
Genes not detected in specific clf disrupted loop
F
Col-0
H3K27me3
Gene E
Gene F
Gene G
Gene H
clf
H3K27me3
Gene E
Gene F
Gene G
Gene H
Col-0
clf
G
Pairs repressed in clf
Pairs induced in clf
LFC2
4
2
0
-2
-3
0
3
6
9
LFC1
(X²) Value = 214.297,
p= 4.33e-7
H
-2
0
2
2.04
1.07
-1.05
Hypo (H3K27me3)
1.29
2.38
-2.38
Up
-1.29
-2.38
2.38
Down
Hypo (H3K27me3)
Up
Down
I
Observed
Expected
(1000 permutations)
40%
60%*
61%
39%
p-value = 1e-03*
J
Genes
CYP702A2
CYP702A3
CSLB06
CYP705A1
PEN1
CYP705A2
CYP705A3
PEN2
CYP705A4
AT4G15390
CYP702A5
CYP702A5
CYP702A5
CYP702A6
AT4G15400
PUX5
8740K
8750K
8760K
8770K
8780K
8790K
8800K
8810K
Col-0 H3K27me3
[0-15]
Col-0 H3K9ac
[20-100]
Col-0 C-HiC
clf H3K27me3
[0-15]
clf H3K9ac
[20-100]
clf C-HiC
Genes
AT4G13110
AT4G13130
AT4G13150
AT4G13100
AT4G13160
AT4G13170
AT4G13180
AT4G13190
CLE44
AT4G13200
AT4G13210
AT4G13220
7630K
7640K
7650K
7660K
7670K
Col-0 H3K27me3
[0-20]
Col-0 H3K9ac
[25-150]
Col-0 C-HiC
clf H3K27me3
[0-20]
clf H3K9ac
[25-150]
clf C-HiC
K
Col-0
clf
Col-0
clf

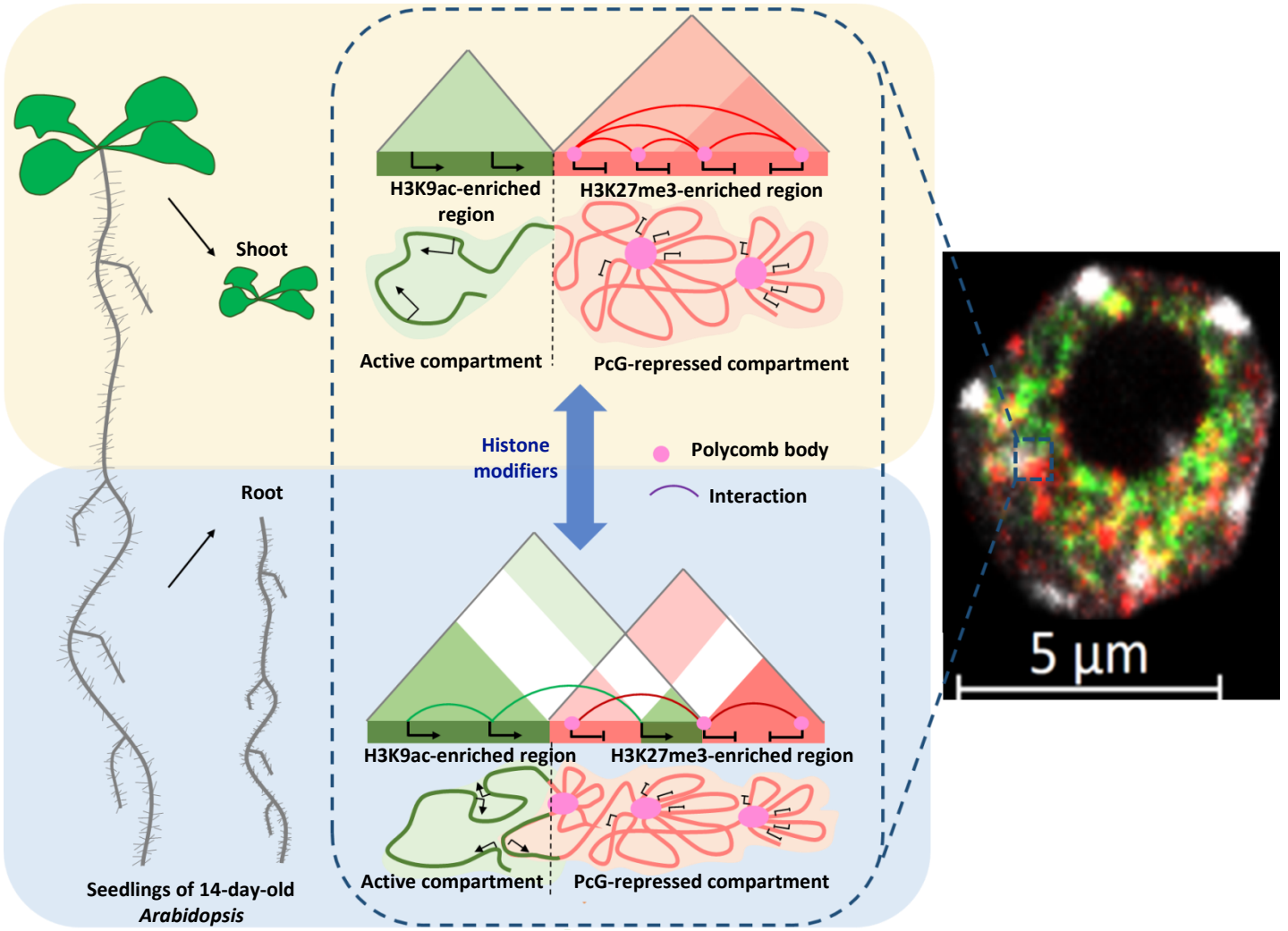
Shoot
Root
Seedlings of 14-day-old
Arabidopsis
H3K9ac-enriched region
H3K27me3-enriched region
Active compartment
PcG-repressed compartment
Histone modifiers
Polycomb body
Interaction
H3K9ac-enriched region
H3K27me3-enriched region
Active compartment
PcG-repressed compartment
5 μm

Supplemental Figure legends

Supplemental Fig S1. Immunofluorescence detection of H3K9ac (green) and H3K27me3 (red) chromatin histone modifications and DAPI staining in isolated *Arabidopsis* nuclei. Three independent nuclei are shown, complementary to Figure 1A.

Supplemental Fig S2. Schematic representation of the HiChIP method.

Supplemental Fig S3. PCA (principal component analysis) plot for different replicates of HiChIP-shoot and root of wild-type *Arabidopsis*. High reproducibility is observed between the replicates in HiChIP experiments.

Supplemental Fig S4. Plots representing the H3K9ac (A) and H3K27me3 (B) chromatin loop size distribution.

Supplemental Fig S5. Visualization of the interaction matrix of HiChIP in shoot and root of wild-type in *Arabidopsis* Chromosome 3. An example of H3K27me3 HiChIP loops showing stronger interactions in shoot compared to root (SSRLs). A shoot loop showing higher signal of H3K27me3 in shoot than root is indicated in the map. ChIP-seq signals of H3K27me3 in shoot and root are shown as blue peaks.

Supplemental Fig S6. Visualization of the interaction matrix of HiChIP in shoot and root of wide-type in *Arabidopsis* Chromosome 3. An example of H3K27me3 HiChIP loops showing stronger interactions in root than in shoot. A root loop showing higher signal of H3K27me3 in root than shoot is indicated in the map. ChIP-seq signals of H3K27me3 in shoot and root are shown as blue peaks.

Supplemental Fig S7. Gene pairs connected in shoot specific repressive loops (SSRL) and root specific repressive loops (RSRL) in *Arabidopsis* wide-type. A higher number of gene pairs are repressed in SSRLs than expected randomly (p-value: 4E-175). For RSRLs, a higher number of gene pairs are induced (log FC shoot/root) than expected randomly (p-value: 3.2E-55).

Supplemental Fig S8. Schematic representation of the Capture Hi-C (C-Hi-C) method.

Supplemental Fig S9. PCA (principal component analysis) plot for different replicates of Capture Hi-C in *Arabidopsis* wild-type shoot and root. High reproducibility was observed between the replicates in Capture Hi-C experiments.

Supplemental Fig S10. (A) Pie chart representing the observed and expected proportion of repressed genes in shoot (blue), repressed genes in root (red) and unchanged (grey) among the genes involved in loops detected both with HiChIP and C-Hi-C. (B) Pie chart representing the observed and expected proportion of repressed genes in shoot (blue), repressed genes in root (red) and unchanged (grey,) among the genes involved in loops detected both with HiChIP and C-Hi-C. To obtain the expected proportion, we shuffled the gene expression value 1000 times to obtain the randomized gene counts. The mean of the 1000 permutations was used to determine the expected proportions.

Supplemental Fig S11. PCA (principal component analysis) plots for different replicates of Capture Hi-C experiments of *ref6-5* mutant and wild-type shoot in *Arabidopsis*. A high reproducibility was observed between the replicates in Capture Hi-C experiments.

Supplemental Fig S12. Gene pairs connected in *ref6-5* specific loops (reSL) in *ref6-5* mutant compared to wild-type shoot in *Arabidopsis*. A higher number of gene pairs are repressed in reSLs than expected by chance (p-value = 4E-10).

Supplemental Fig S13. PCA (principal component analysis) plot for different replicates of *clf* mutant and *Arabidopsis* wild-type. A high reproducibility was observed between the replicates in Capture Hi-C experiments.

Supplemental Fig S14. Gene pairs connected in *clf* destabilized loops in *clf* mutant. A higher number of gene pairs are induced than expected randomly (p-value: 4.33E-7).

Supplemental Fig S15. Examples of important developmental genes *AGAMOUS* (*AG*), *AGL24*, *WRKY14* and *CYCB1;5* losing H3K27me3 in *clf* and that tend to establish interactions with regions marked with

H3K9ac euchromatin mark. C-Hi-C interactions (blue lines), H3K9ac ChIP-seq signal in wild-type and *clf* (green peaks), H3K27me3 ChIP-seq signal in wild-type and *clf* (red peaks) are represented, respectively.

Supplemental Fig S16. Hypomethylated gene pairs interacting in *clf* are associated with H3K9ac. A density plot shows that interacting gene pairs in *clf,* which are hypomethylated, are also associated with the active histone modification H3K9ac in wild-type *Arabidopsis*. The frequency of observed Hypo-H3K27me3 and H3K9ac interactions is 60% and is greater than the expected frequency over 1000 permutations (39%).

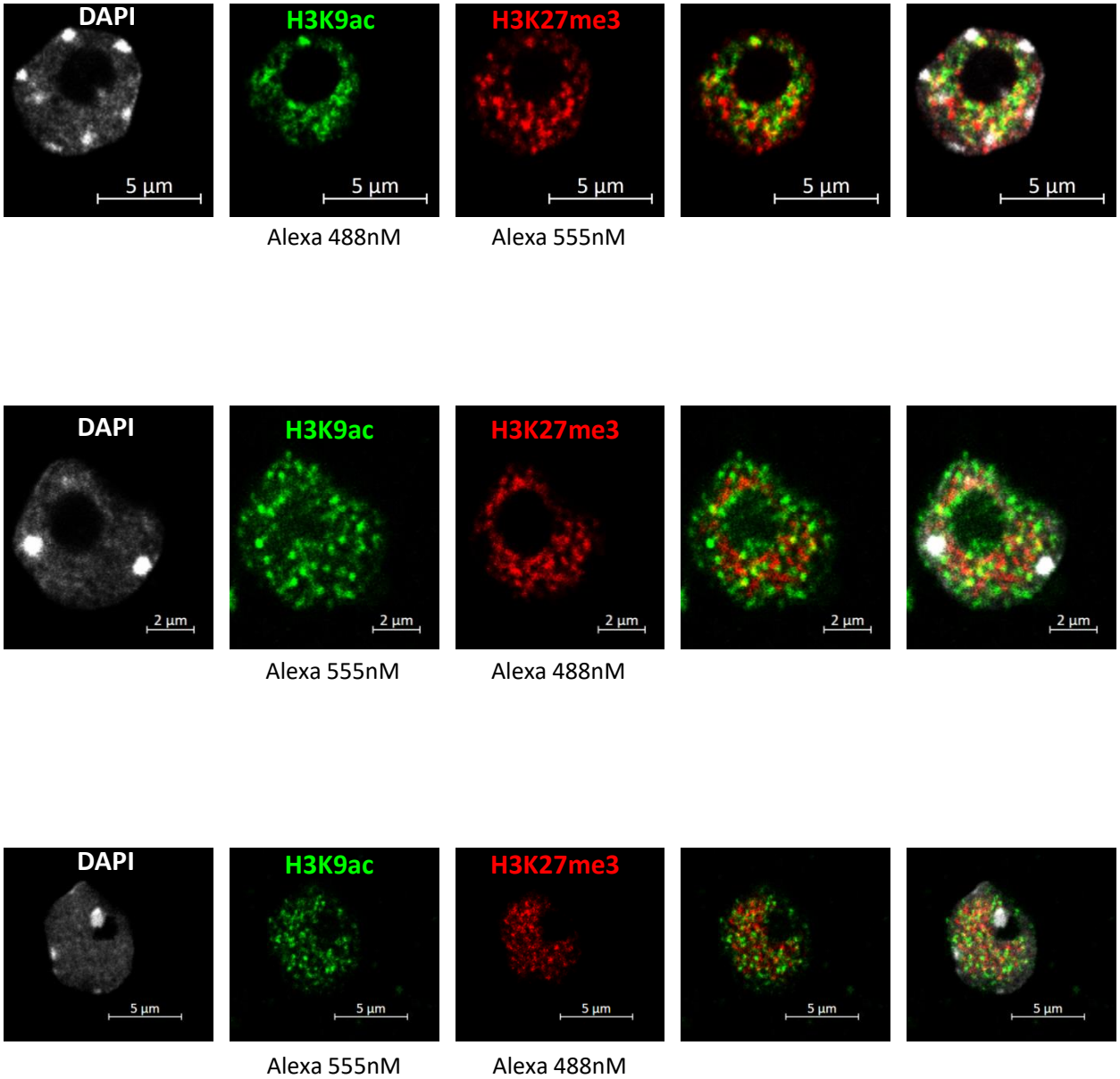

Supplemental Fig S1. Immunofluorescence detection of H3K9ac (green) and H3K27me3 (red) chromatin marks and DAPI staining in isolated *Arabidopsis* nuclei. Three independent nuclei are shown, complementary to Figure 1A.

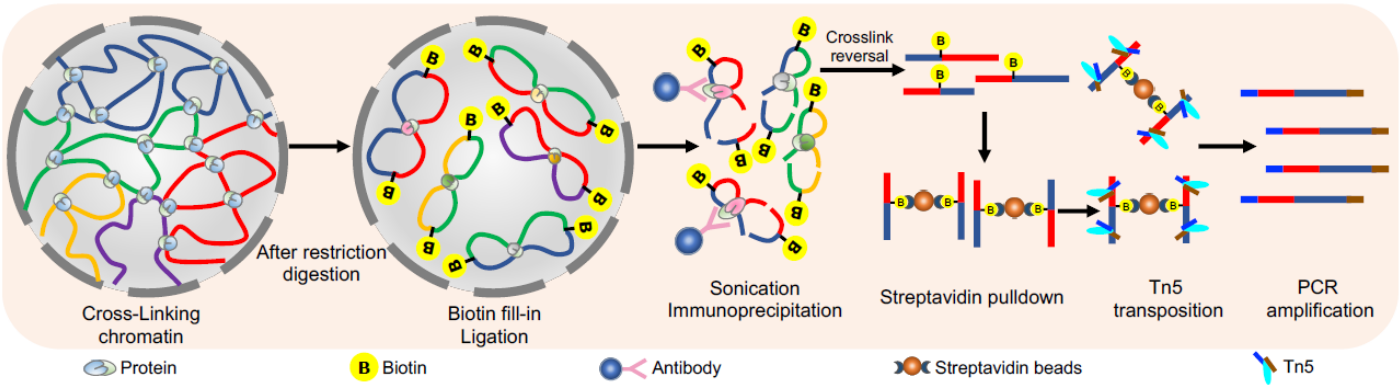

Supplemental Fig S2. Schematic representation of the HiChIP method.

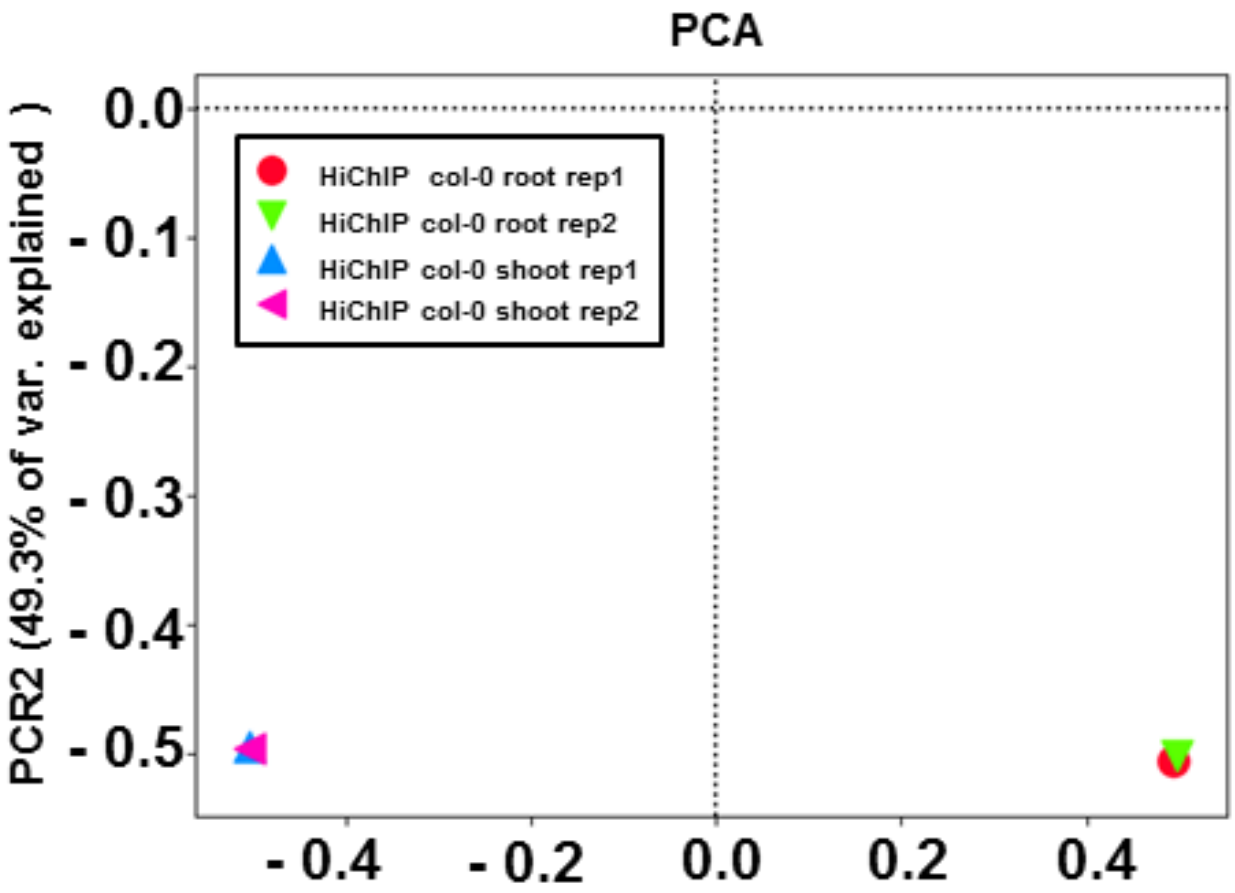

Supplemental Fig S3. PCA (principal component analysis) plot for different replicates of HiChIP-shoot and root of wild-type *Arabidopsis*. High reproducibility is observed between the replicates in HiChIP experiments.

A

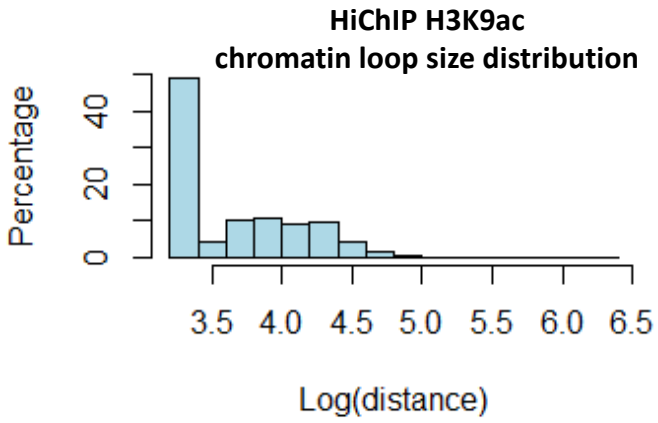

B

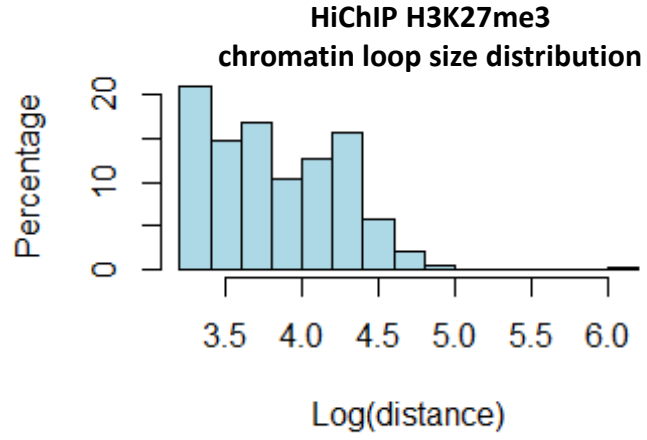

Supplemental Fig S4. Plots representing the H3K9ac **(A)** and H3K27me3 **(B)** chromatin loop size distribution

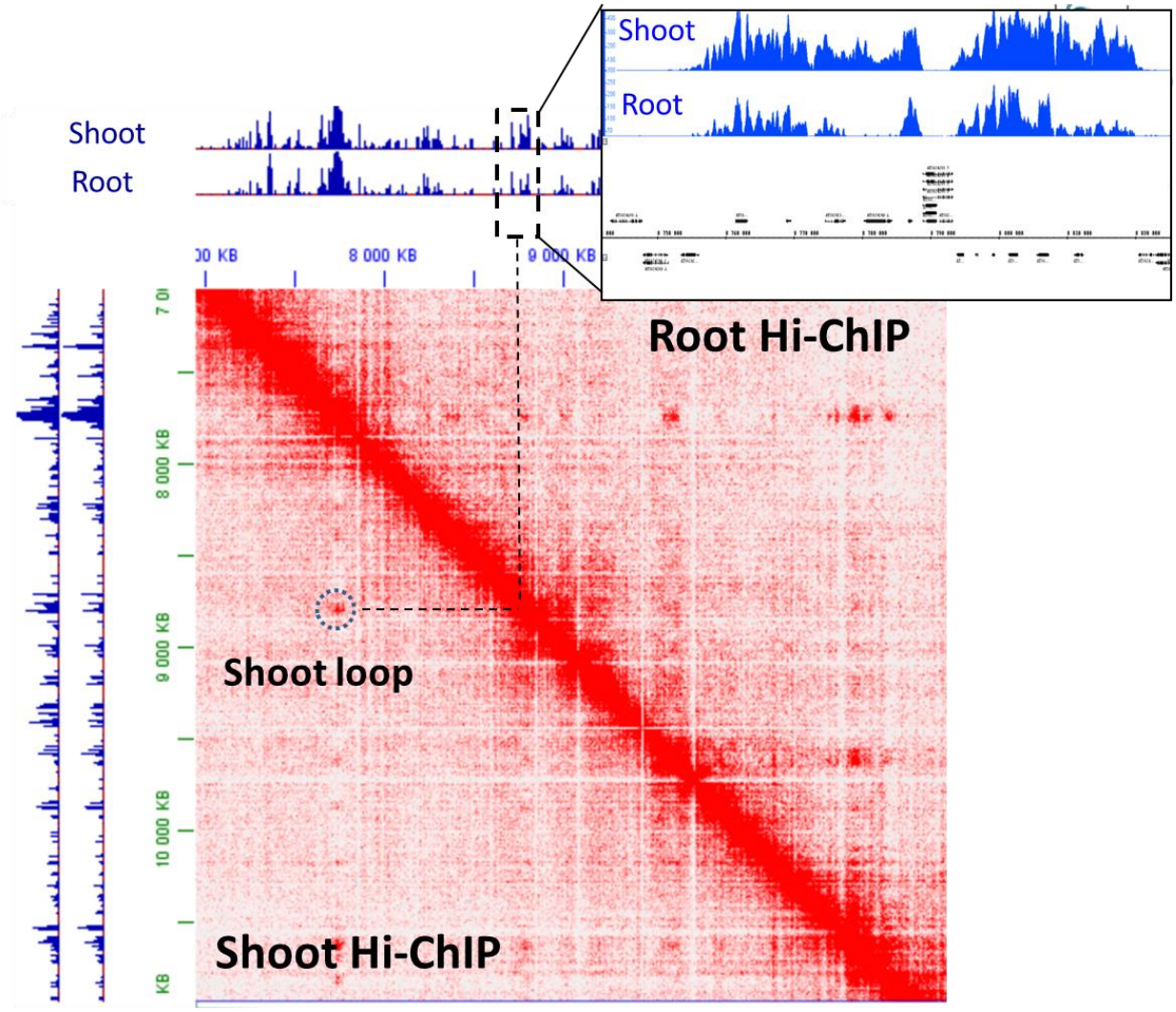

Supplemental Fig S5. Visualization of the interaction matrix of HiChIP in shoot and root of wild-type in *Arabidopsis* Chromosome 3 . An example of H3K27me3 HiChIP loops showing stronger interactions in shoot compared to root (SSRLs). A shoot loop showing higher signal of H3K27me3 in shoot than root is indicated in the map. ChIP-seq signals of H3K27me3 in shoot and root are shown as blue peaks.

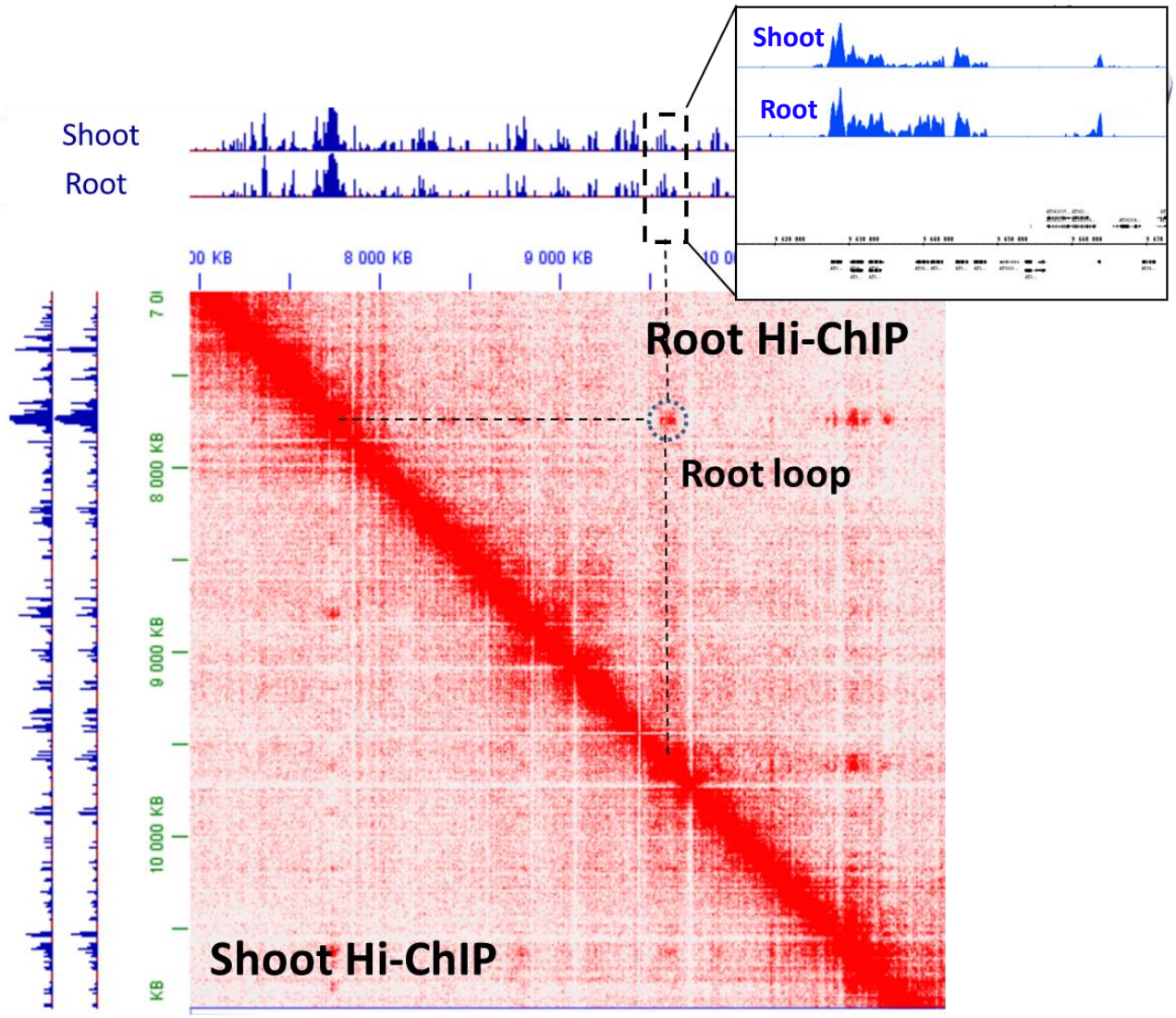

Supplemental Fig S6. Visualization of the interaction matrix of HiChIP in shoot and root of wide-type in *Arabidopsis* Chromosome 3. An example of H3K27me3 HiChIP loops showing stronger interactions in root than in shoot. A root loop showing higher signal of H3K27me3 in root than shoot is indicated in the map. ChIP-seq signals of H3K27me3 in shoot and root are shown as blue peaks.

A

Shoot specific repressive loops (SSRL)	**Gene1-Log FC >0 induced**	**Gene1-Log FC_1<0 repressed**
Gene2-Log FC >0 induced	**194**	362
Gene2-Log FC_1<0 repressed	411	**1033***

X^2 (3, N = 2000) = 809.38, p = 4.0E-175

B

Root specific repressive loops (RSRL)	**Gene1-Log FC >0 induced**	**Gene1-Log FC_1<0 repressed**
Gene2-Log FC >0 induced	**801***	443
Gene2-Log FC_1<0 repressed	425	331

X^2 (3, N = 2000) = 256.072, p=3.2E-55

Supplemental Fig S7. Gene pairs connected in shoot specific repressive loops (SSRL) and root specific repressive loops (RSRL) in *Arabidopsis* wide-type. A higher number of gene pairs are repressed in SSRLs than expected randomly (p-value: 4E-175). For RSRLs, a higher number of gene pairs are induced (log FC shoot/root) than expected randomly (p-value: 3.2E-55).

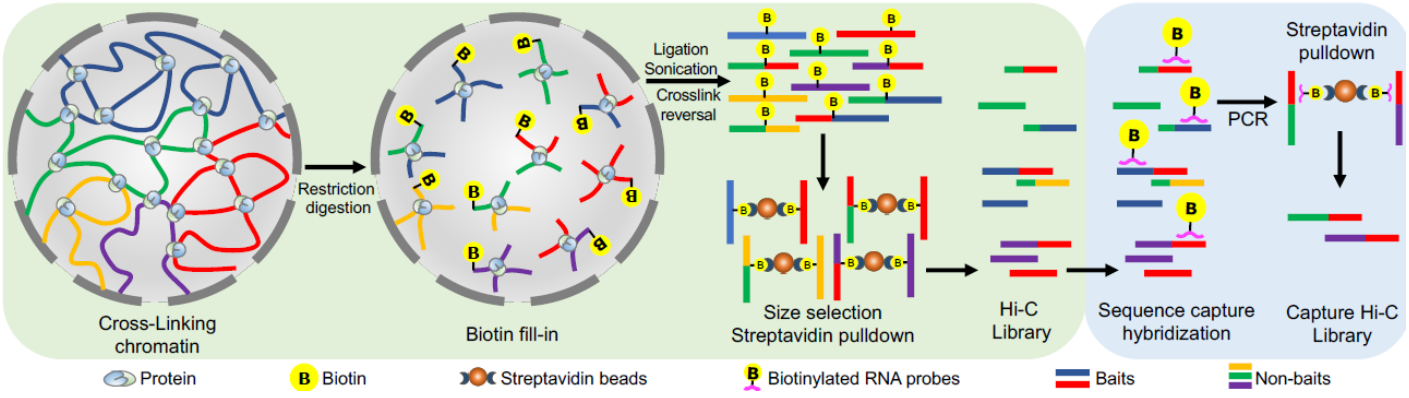

Supplemental Fig S8. Schematic representation of the Capture Hi-C (C-Hi-C) method.

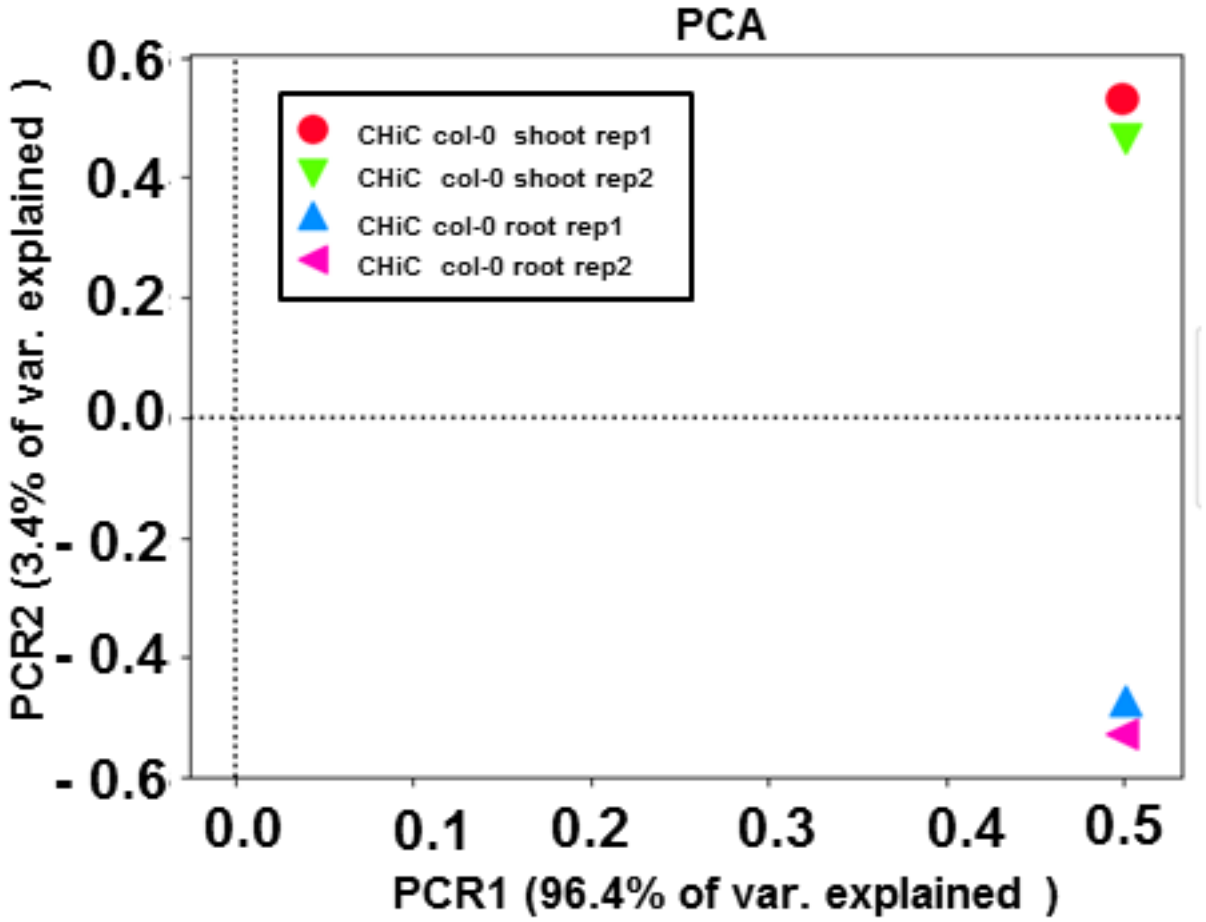

Supplemental Fig S9. PCA (principal component analysis) plot for different replicates of Capture Hi-C in *Arabidopsis* wild-type shoot and root. High reproducibility was observed between the replicates in Capture Hi-C experiments.

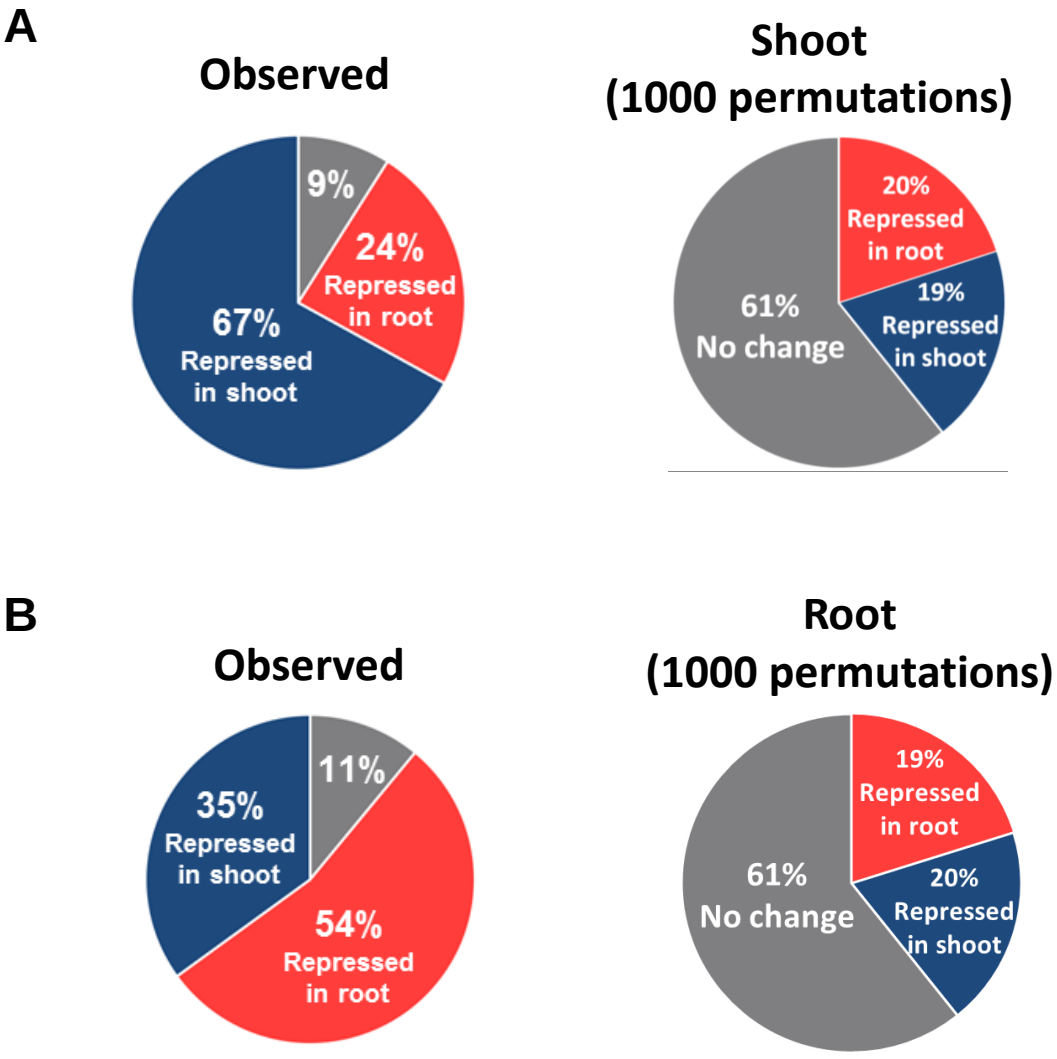

Supplemental Fig S10. (A) Pie chart representing the observed and expected proportion of repressed genes in shoot (blue), repressed genes in root (red) and unchanged (grey) among the genes involved in loops detected both with HiChIP and C-Hi-C. **(B)** Pie chart representing the observed and expected proportion of repressed genes in shoot (blue), repressed genes in root (red) and unchanged (grey,) among the genes involved in loops detected both with HiChIP and C-Hi-C.
To obtain the expected proportion, we shuffled the gene expression signals 1000 times to obtain a randomized one. The mean of the 1000 permutations was used to determine the expected proportions.

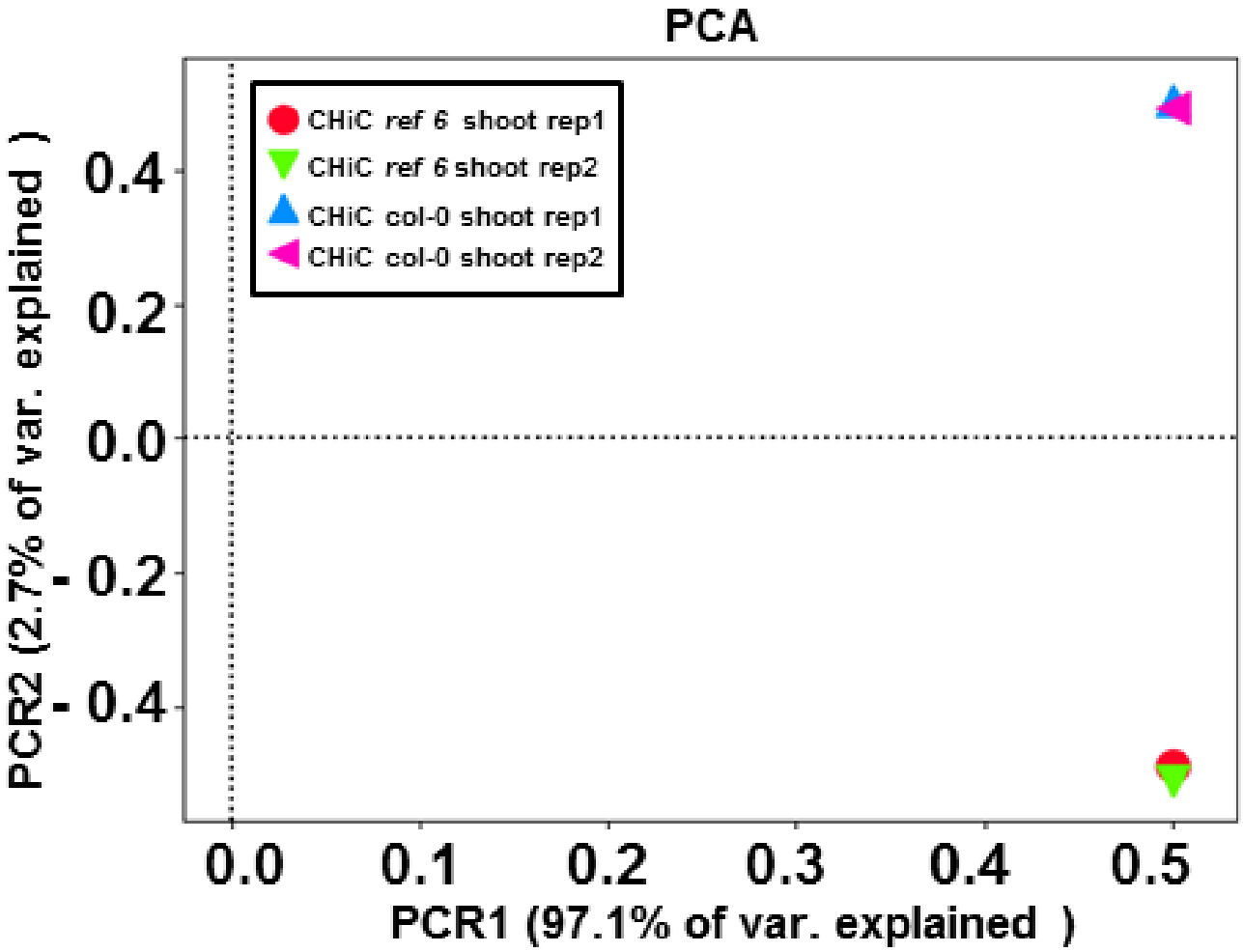

Supplemental Fig S11. PCA (principal component analysis) plots for different replicates of Capture Hi-C experiments of *ref6-5* mutant and wild-type shoot in *Arabidopsis*. A high reproducibility was observed between the replicates in Capture Hi-C experiments.

Interactions gained in *ref6-5*	Gene1-Log FC >0 induced	Gene1-Log FC_1<0 repressed
Gene2-Log FC >0 induced	**117**	116
Gene2-Log FC_1<0 repressed	113	**200***

X^2 (3, N = 2000) = 39.1, p = 4E-10

Supplemental Fig S12. Gene pairs connected in *ref6-5* specific loops (reSL) in *ref6-5* mutant compared to wild-type shoot in *Arabidopsis*. A higher number of gene pairs are repressed in reSLs than expected by chance (p-value = 4E-10).

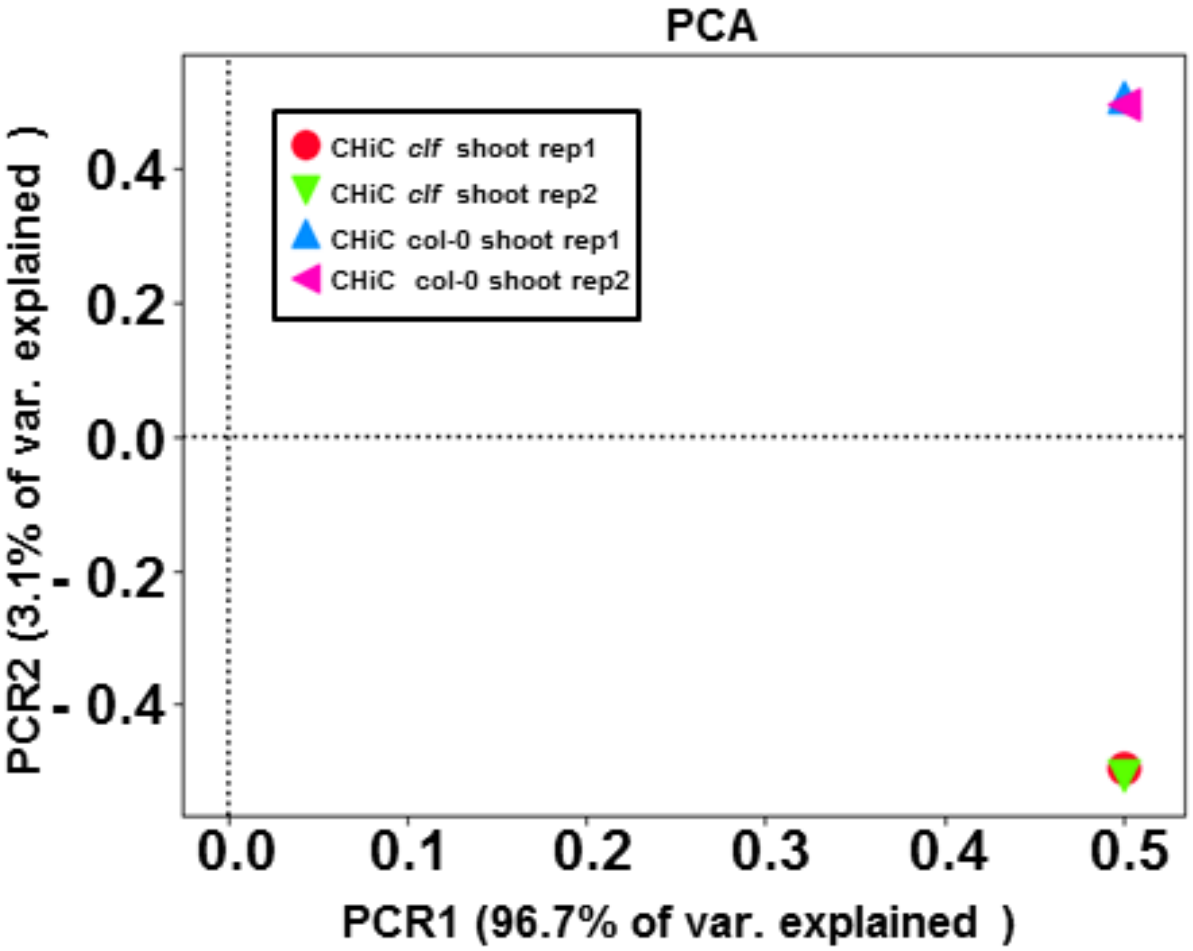

Supplemental Fig S13. PCA (principal component analysis) plot for different replicates of *clf* mutant and *Arabidopsis* wild-type. A high reproducibility was observed between the replicates in Capture Hi-C experiments.

Interactions lost in *clf*	Gene1-Log FC >0 induced	Gene1-Log FC_1<0 repressed
Gene2-Log FC >0 induced	**185***	43
Gene2-Log FC_1<0 repressed	43	30

$$X^2\ (3,\ N = 2000) = 214.297,\ p = 4.33E\text{-}7$$

Supplemental Fig S14. Gene pairs connected in *clf* destabilized loops in *clf* mutant. A higher number of gene pairs are induced than expected randomly (p-value: 4.33E-7).

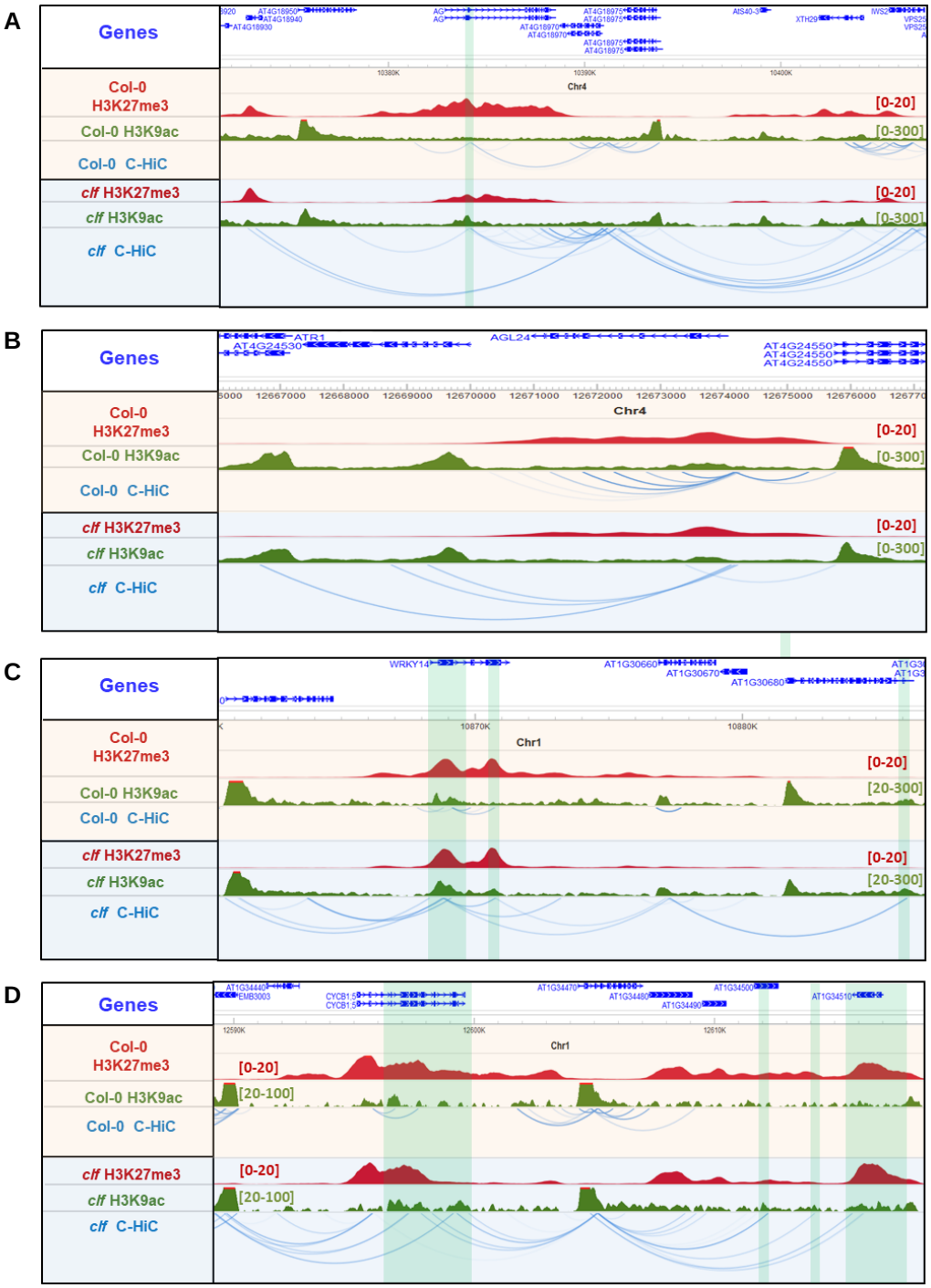

Supplemental Fig S15. Examples of important developmental genes AGAMOUS (AG), AGL24, WRKY14 and CYCB1;5 losing H3K27me3 in *clf* and that tend to establish interactions with regions marked with H3K9ac euchromatin mark. C-Hi-C interactions (blue lines), H3K9ac ChIP-seq signal in wild-type and *clf* (green peaks), H3K27me3 ChIP-seq signal in wild-type and *clf* (red peaks) are represented, respectively.

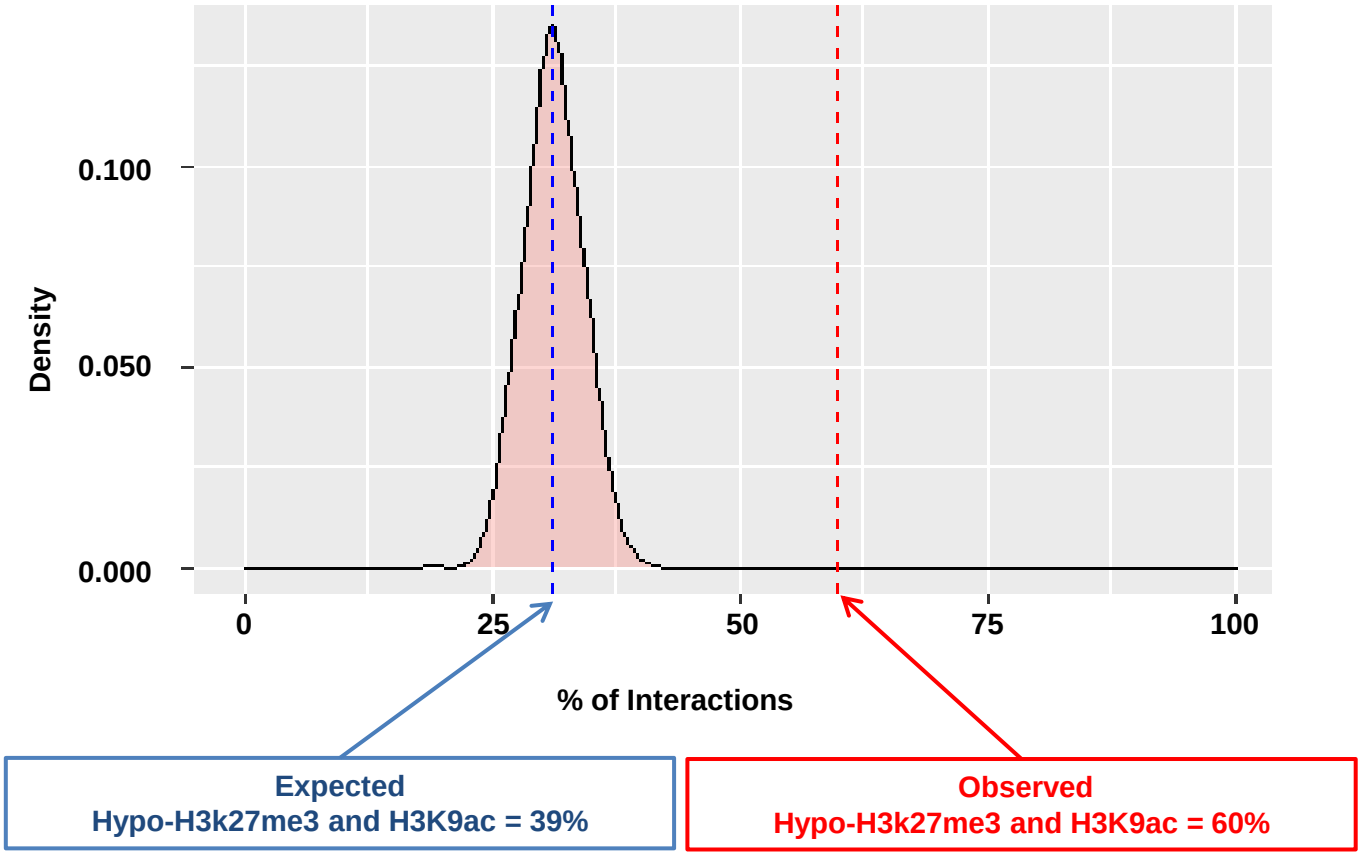

Supplemental Fig S16. Hypomethylated gene pairs interacting in *clf* are associated with H3K9ac. A density plot shows that interacting gene pairs in *clf,* which are hypomethylated, are also associated with the active mark H3K9ac in wild-type *Arabidopsis*. The frequency of observed Hypo-H3K27me3 and H3K9ac interactions is 60% and is greater than the expected frequency over 1000 permutations (39%).